Molecular subclasses of high-grade glioma predict prognosis, delineate a pattern of disease progression, and resemble stages in neurogenesis

Heidi S. Phillips,[1,*] Samir Kharbanda,[1] Ruihuan Chen,[1] William F. Forrest,[2] Robert H. Soriano,[3] Thomas D. Wu,[4] Anjan Misra,[5] Janice M. Nigro,[5] Howard Colman,[6] Liliana Soroceanu,[1] P. Mickey Williams,[3] Zora Modrusan,[3] Burt G. Feuerstein,[5] and Ken Aldape[7]

[1] Department of Tumor Biology and Angiogenesis, Genentech, Inc., South San Francisco, California 94080
[2] Department of Biostatistics, Genentech, Inc., South San Francisco, California 94080
[3] Department of Molecular Biology, Genentech, Inc., South San Francisco, California 94080
[4] Department of Bioinformatics, Genentech, Inc., South San Francisco, California 94080
[5] Brain Tumor Research Center, University of California, San Francisco, San Francisco, California 94143
[6] Department of Neuro-Oncology, M.D. Anderson Cancer Center, Houston, Texas 77030
[7] Department of Pathology, M.D. Anderson Cancer Center, Houston, Texas 77030
*Correspondence: hsp@gene.com

Summary

Previously undescribed prognostic subclasses of high-grade astrocytoma are identified and discovered to resemble stages in neurogenesis. One tumor class displaying neuronal lineage markers shows longer survival, while two tumor classes enriched for neural stem cell markers display equally short survival. Poor prognosis subclasses exhibit markers either of proliferation or of angiogenesis and mesenchyme. Upon recurrence, tumors frequently shift toward the mesenchymal subclass. Chromosomal locations of genes distinguishing tumor subclass parallel DNA copy number differences between subclasses. Functional relevance of tumor subtype molecular signatures is suggested by the ability of cell line signatures to predict neurosphere growth. A robust two-gene prognostic model utilizing PTEN and DLL3 expression suggests that Akt and Notch signaling are hallmarks of poor prognosis versus better prognosis gliomas, respectively.

Introduction

High-grade gliomas (HGGs), which include glioblastoma (GBM) and anaplastic astrocytoma (AA), are the most common intrinsic brain tumors in adults and are nearly uniformly fatal. While there has been progress in understanding the molecular genetics of these tumors (Kitange et al., 2003), the cell type(s) of origin are still uncertain, and the molecular determinants of disease aggressiveness are not well understood. A better understanding of the cellular origin and molecular pathogenesis of these tumors may identify new targets for treatment of these neoplasms.

Until recently, HGGs were presumed to arise from glial cells residing within the brain parenchyma. However, recent evidence in human and animal studies suggests neural stem cells as an alternate cellular origin of gliomas (Caussinus and Gonzalez, 2005; Singh et al., 2003; Zhu et al., 2005). Mouse models demonstrate that astrocytes or neural stem/progenitor cells can give rise to neoplasms that recapitulate the histopathological hallmarks of human gliomas (Bachoo et al., 2002; Uhrbom et al., 2002). Demonstrations that the adult human forebrain contains an abundant source of neural stem cells (Sanai et al., 2004) and that human GBMs contain tumorigenic neural stem-like cells (Galli et al., 2004; Ignatova et al., 2002; Singh et al., 2004) indicate that neural stem and/or progenitor cells are a plausible origin for human gliomas and have given rise to speculation that more effective therapies will result from approaches aimed at targeting the stem cell-like component of GBM (Berger et al., 2004; Fomchenko and Holland, 2005; Ignatova et al., 2002; Oliver and Wechsler-Reya, 2004). Importantly, however, the contribution of stem-like cells to disease progression or therapeutic response has not been established, nor is it clear what proportion of tumor cells exhibit stem-like properties.

SIGNIFICANCE

Recent evidence suggests that gliomas may arise from a cell type with neural stem cell-like properties. The current work demonstrates that prognostic subtypes of glioma resemble key stages in neurogenesis and implicates signaling pathways that play critical roles in regulation of forebrain neurogenesis in control of tumor aggressiveness. Longitudinal analysis of glioma cases reveals a frequent pattern of disease progression into the mesenchymal phenotype, a state associated with robust angiogenesis. This work suggests that molecular classification of glioblastoma may predict response to targeted therapies and suggests that greater understanding of neurogenesis in the adult forebrain may yield novel therapeutic insights for glial malignancies.

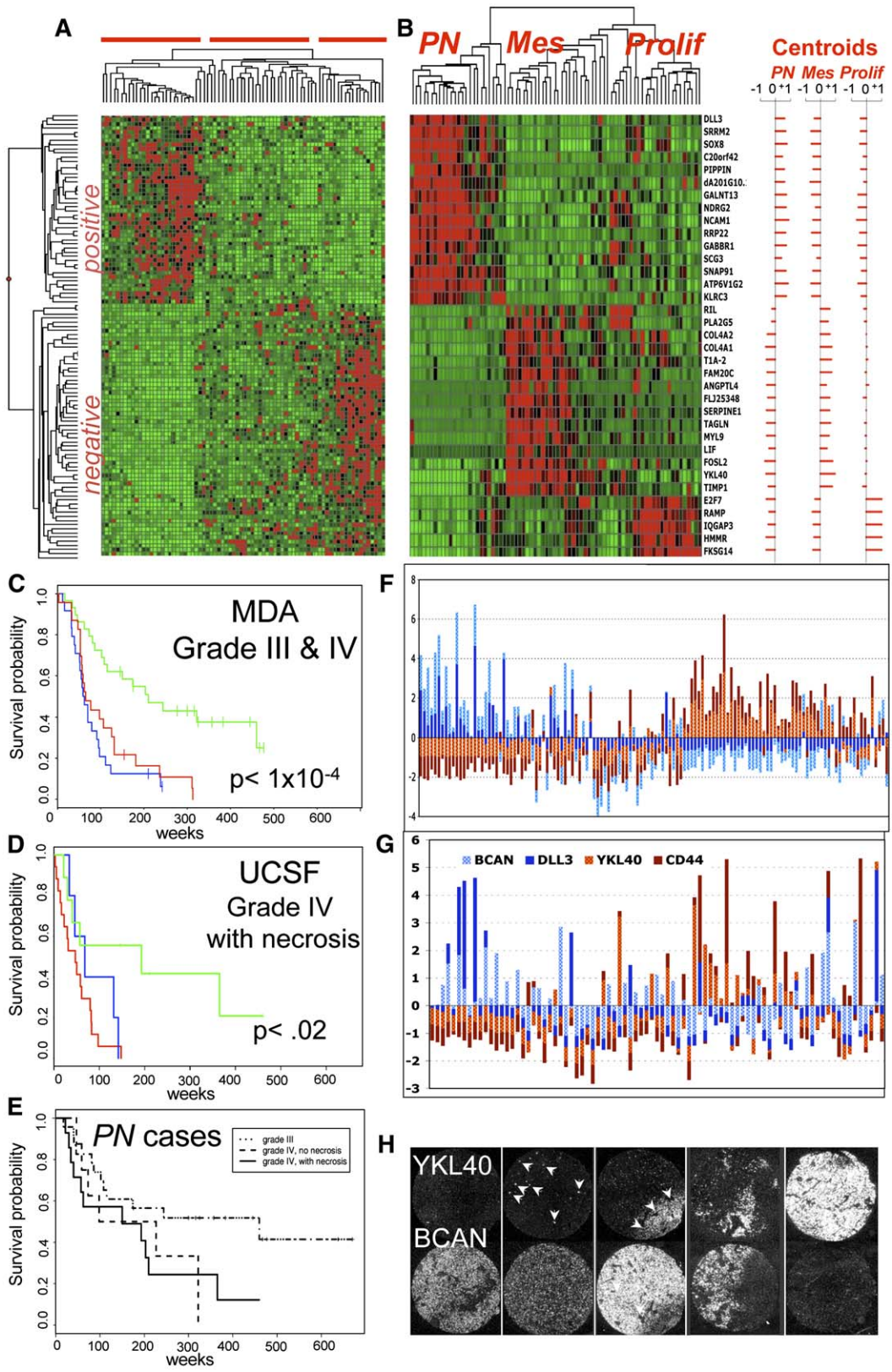

Figure 1. Expression profiling reveals three major patterns of gene expression related to survival in HGG

A: Unsupervised clustering of 76 primary astrocytomas by expression of 108 genes positively or negatively correlated with survival (gene clusters labeled positive or negative) reveals three sample clusters (red lines).

B: *PN*, *Prolif*, and *Mes* tumor subsets are identified using 35 signature genes. Centroids from k-means clustering are depicted using Z score-normalized gene expression values (scale from −1 to +1).

Several studies have investigated molecular correlates of prognosis and clinical subclasses in AA and GBM (also known as grade III and IV astrocytoma, respectively). Tumor grade is the most established and robust predictor of disease outcome (Prados and Levin, 2000). Loss of chromosome (chr) 10q is a more frequent occurrence in GBM than AA and has been associated with short GBM survival (Balesaria et al., 1999; Schmidt et al., 2002; Smith et al., 2001). While *p53* mutation and *EGFR* amplification reportedly define mutually exclusive GBM subgroups (von Deimling et al., 1995; Watanabe et al., 1996), a recent study challenges the validity of this classification scheme (Okada et al., 2003), and the prognostic value of either *p53* mutation or alterations of the *EGFR* locus is not clear (Heimberger et al., 2005; Ushio et al., 2003).

Microarray expression profiling of gliomas has identified molecular subtypes as well as genes associated with tumor grade, progression, and patient survival (Godard et al., 2003; Rickman et al., 2001; van den Boom et al., 2003). While GBM and AA continue to be defined by histological criteria, reports that expression profiles predict outcome better than histological class (Freije et al., 2004; Nutt et al., 2003) provide support for the hypothesis that neoplasms defined morphologically as AA and GBM represent a mix of molecular genetic subtypes. Given the possibility that molecularly distinct disease entities may exhibit different clinical responses, a greater understanding of the behavior of molecularly defined subsets of tumors may aid in the development of more effective therapies.

Efforts to develop targeted therapies for glial malignancies have been hampered by complexities arising from intratumoral and intertumoral molecular heterogeneity. An additional challenge in the management of gliomas is the nearly universal propensity of these neoplasms to contain cells that survive surgery and radiation therapy and form recurrent lesions that are resistant to further treatment. Methods to classify tumors according to key molecular events that regulate growth of their most aggressive cellular component and to predict changes that accompany disease recurrence might greatly facilitate development of targeted therapies. In the current study, we identify molecular subclasses of high-grade astrocytoma with prognostic value, relate these tumor subtypes to activation of signaling pathways, and identify changes in gene expression that commonly accompany recurrence. Parallels between the prognostic tumor subclasses identified in this study and stages in the differentiation of neural stem cells suggest that aggressiveness of HGGs is regulated by processes similar to those that control forebrain neurogenesis.

Results

Molecular signatures define prognostic subclasses of high-grade astrocytoma

Seventy-six samples from newly diagnosed cases of WHO grade III and IV astrocytomas from M.D. Anderson Cancer Center (MDA) were profiled via DNA microarrays to identify gene expression patterns that classify tumors into prognostic groups (Figures 1A–1C). All tumor cases analyzed are described in Table S1 in the Supplemental Data available with this article online. We first identified probe sets whose expression most strongly correlated with survival (Spearman r of log-transformed expression intensity values versus survival times >0.45 or <−0.45), followed by two-way agglomerative clustering of the 108 resulting probe sets and 76 samples. This analysis identified three discrete groups of sample sets that differ markedly in their expression of the survival-related genes (Figure 1A).

In order to define markers for each of the three tumor subclasses, we identified probe sets most strongly overexpressed by each tumor subgroup as compared to remaining subclasses (see Table S3). Using the most robust markers for each of the three tumor subsets, we derived a set of 35 genes, referred to as signature genes, that can be used in either hierarchical clustering (Figure 1B) or k-means clustering to assign tumors to subclass. The HGG subclasses defined by k-means clustering are designated proneural (*PN*), proliferative (*Prolif*) and mesenchymal (*Mes*) to recognize the dominant feature of the gene list that characterizes each subclass. For each tumor subclass, a centroid was calculated from the average expression values of the 35 signature genes (Figure 1B). A centroid can be viewed as the prototypical expression pattern for a tumor subtype, and additional samples can be classified by similarity of signature gene expression to these centroids. Kaplan-Meier plots for cases in the MDA data set showed that median survival of the *PN* subclass (174.5 weeks) was markedly longer than either *Prolif* (60.5) or *Mes* subtypes (65.0 weeks; Figure 1C). Classification of a published data set of HGG (Freije et al., 2004) by similarity to centroids defined by the MDA data set revealed very similar differences in survival between *PN* tumors and the other subclasses (Table S1; Figure S1).

To determine if this classification scheme has prognostic value independent of tumor grade, we utilized an additional independent set of 31 cases treated at University of California San Francisco (UCSF). These tumors, all WHO grade IV astrocytomas with necrosis, were classified as *PN*, *Prolif*, or *Mes* by similarity of signature gene expression to centroids defined by the MDA data set (Table S6). Significant prognostic value of molecular classification was seen within this set of histologically uniform HGGs (Figure 1D). In addition, application of a multivariate Cox model to a combined data set containing a total of 115 grade III and grade IV astrocytomas from MDA and UCSF (Table S1) revealed that tumor subtype has significant prognostic value ($p < 0.02$) that is independent of WHO tumor grade and/or the presence of necrosis, a variable within GBMs that is reported to correlate with survival (Barker et al., 1996).

We next compared expression of selected *PN* and *Mes* markers by both microarray and quantitative real-time PCR (qPCR). We chose delta-like ligand 3 (DLL3) and CHI3L1/YKL-40 (YKL40) as *PN* and *Mes* markers, respectively, from the signature gene list and brevican (BCAN) and CD44 from the more extensive list of markers (Table S3) for these same

C and D: Kaplan-Meier plots showing survival of all MDA cases (**C**) or of UCSF grade IV cases with necrosis (**D**). p values from log-rank tests shown. Green, blue, and red lines correspond to *PN*, *Prolif*, and *Mes* subclasses, respectively. Vertical ticks indicate censored survival observations.
E: Survival of *PN* HGG as a function of histological grade.
F and G: Strong expression of *PN* markers and strong expression of *Mes* markers are mutually exclusive. Each bar depicts mRNA determinations by microarray (**F**) or TaqMan real-time PCR (**G**) of four marker genes in an individual sample. Genes include BCAN, DLL3, YKL40, and CD44 as indicated. Values displayed represent Z scores for gene expression of individual samples relative to the entire sample set.
H: In situ hybridization of BCAN and YKL40 in tissue microarray cores of five glioma cases. Arrows indicate focal YKL40 expression in BCAN-positive cores.

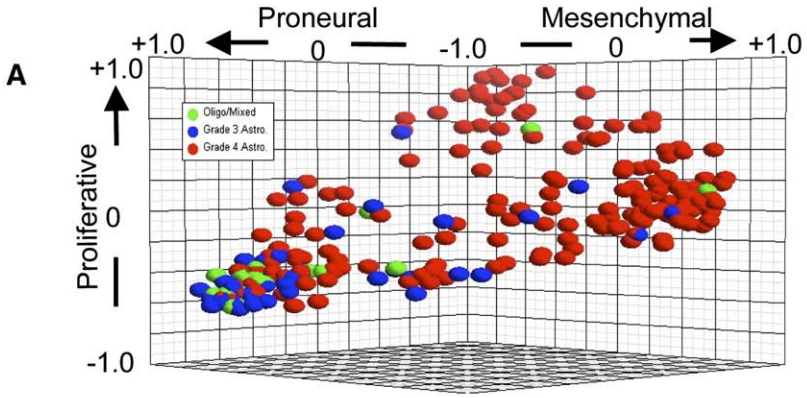

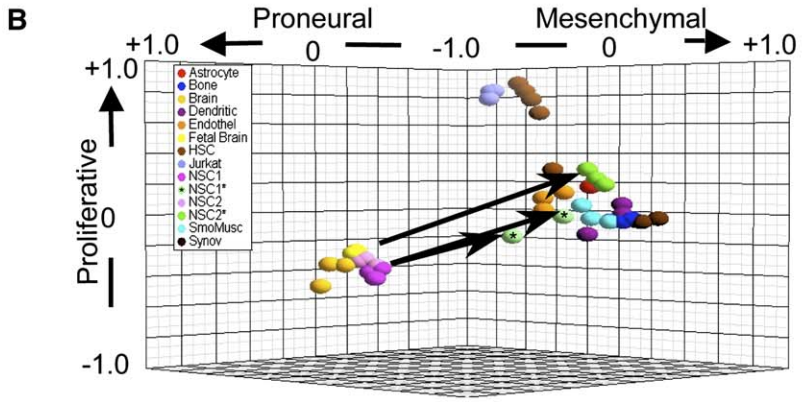

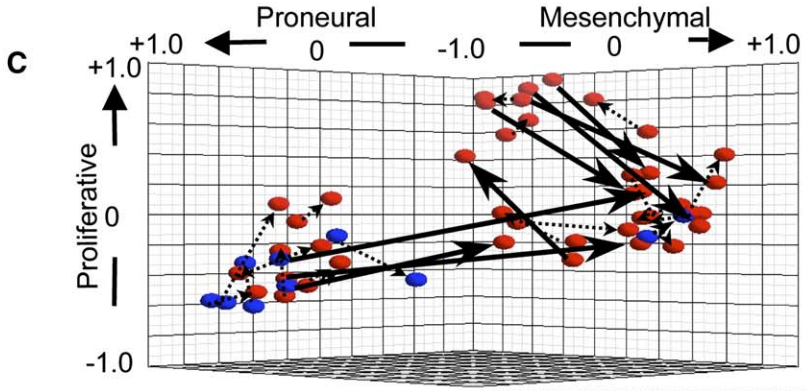

D

Affy ID	Gene	FC			
211530_x_at	HLA-G	4.4	(cont.)		
209396_s_at	CHI3L1/YKL40	4.3	200660_at	S100A11	2.3
202628_s_at	SERPINE1	4.3	200808_s_at	ZYX	2.2
203963_at	CA12	3.8	208540_x_at	S100A11P	2.2
209395_at	CHI3L1/YKL40	3.6	204489_s_at	CD44	2.2
202627_s_at	SERPINE1	3.6	221881_s_at	CLIC4	2.2
215867_x_at	CA12	3.5	200742_s_at	TPP1	2.2
212014_x_at	CD44	3.4	200656_s_at	P4HB	2.1
201666_at	TIMP1	3.3	IBRDC3(p)	IBRDC3(p)	2.0
214164_x_at	CA12	3.1	201325_s_at	EMP1	2.0
209835_x_at	CD44	2.9	211529_x_at	HLA-G	1.9
204490_s_at	CD44	2.7	201324_at	EMP1	1.8
210916_s_at	CD44	2.7	209875_s_at	SPP1	1.8
208637_x_at	ACTN1	2.7	200803_s_at	TEGT	1.7
200986_at	SERPING1	2.5	200983_x_at	CD59	1.7
218368_s_at	TNFRSF12A	2.4	221962_s_at	UBE2H	1.6
201105_at	LGALS1	2.3	208992_s_at	STAT3	1.6
210514_x_at	HLA-G	2.3	201426_s_at	VIM	1.6
201161_s_at	CSDA	2.3	200634_at	PFN1	1.6

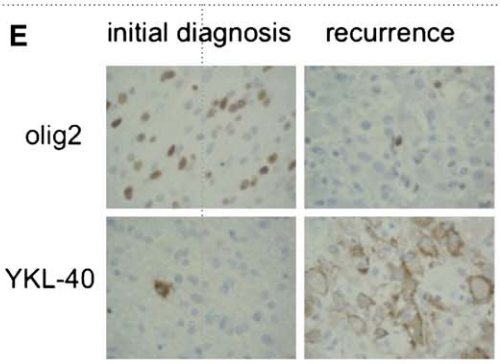

Figure 2. Most HGGs are characterized by strong similarity to one of three patterns of signature gene expression, and subclass shifts upon disease progression are toward the *Mes* phenotype

A–C: Three-dimensional graphical representation in which the position occupied by each point represents the similarity (Spearman r) between an individual sample and each of three centroids defined by k-means clustering of the reference (MDA) sample set. **A:** Nearly all grade III tumors of both astrocytic (blue) or oligodendroglial (green) morphology are most similar to the *PN* centroid, while the population of grade IV tumors (red) is more evenly divided by similarity to

two subclasses, respectively. Most glioma samples displayed expression values above the population mean for either both *PN* markers or both *Mes* markers, but rarely for combinations of *PN* and *Mes* markers (Figures 1F and 1G).

In situ hybridization on a set of independent tumor cases confirmed a mutually exclusive pattern of expression for BCAN and YKL40 mRNAs (Figure 1H). Most specimens displayed strong signal for either BCAN or YKL40, but not both markers. Some specimens did, however, display focal expression of each of the two markers in nonoverlapping cellular elements. Most typically, these were specimens with small foci of YKL40 expression in specimens containing broad BCAN-positive regions. In such cases, YKL40 was frequently expressed in tumor cells associated with blood vessels.

PN, *Prolif*, and *Mes* signatures define tumor subpopulations that differ in tumor grade and patient age

Expanding our analysis to include a total of 256 HGGs (Table S1), we observed that most tumors displayed a strong similarity to one of the three centroids and a neutral or negative correlation with the other two centroids. This finding is reflected by the tendency of samples to cluster at the apices of a triangle in the three-dimensional plot displayed in Figure 2A. While some samples showed intermediate similarity to two centroids, very few samples showed weak or neutral similarities to all three centroids. Thus, most HGGs tend to reside in one of three discrete phenotypic states, and more rarely exist in a condition intermediate between two states.

These HGG subclasses displayed a strong association with histological tumor grade ($p < 1 \times 10^{-14}$, Fisher's exact or chi-square test). Nearly all WHO grade III tumor specimens examined (65/73 or 89%) were classified as *PN* regardless of whether they exhibited oligodendroglial or astrocytic morphology. In contrast, a significant proportion of WHO grade IV lesions (GBM) were classified into each of the three molecular categories. Of 183 GBM samples examined, 31% were *PN*, 20% were *Prolif*, and 49% were *Mes*.

Of the 115 HGG cases fully annotated for histological features, we found that while *PN* HGGs contain a mixture of WHO grade III tumors (AA) as well as WHO grade IV tumors (GBM) with or without necrosis, *Mes* and *Prolif* HGGs are predominantly or exclusively WHO grade IV tumors with necrosis. Of the WHO grade IV cases for which full histology was available, 36% (8/22) of *PN* subtype lacked necrosis, while only 7.5% (3/40) of *Mes* and 0% (0/29) of *Prolif* subtypes lack this feature. Among *PN* HGGs, however, WHO grade IV cases with or without necrosis showed no difference in survival time (log rank $p > 0.80$, Figure 1E).

Consistent with well-established correlations of both tumor grade and survival time to patient age, we found that molecular classification of tumors stratifies patients on the basis of age. Among 185 newly diagnosed cases of HGG (n = 115 MDA and UCSF; n = 70 UCLA; Table S1), *PN* subclass cases were younger than those in either the *Prolif* or *Mes* subclass ($p < 0.005$, Student's t tests for both comparisons). Mean age ± SEM for patients with tumors of *PN*, *Prolif*, and *Mes* subclass was 40.5 ± 1.4 years, 49.0 ± 2.5 years, and 50.7 ± 1.3 years, respectively. For WHO grade IV tumors in this sample set, *Mes* cases were older than *PN* ($p < 0.05$, Student's t test), while *Prolif* cases did not differ in age from either of the other two classes.

PN, *Prolif*, and *Mes* signatures characterize distinct sets of normal tissues

To gain insights into the biological significance of the *PN*, *Prolif*, and *Mes* tumor signatures, we examined expression of the 35 signature genes in several human tissue and cell types. This analysis revealed that distinct sets of tissues resemble each of glioma subclasses (Figure 2B; Table S4). Both fetal and adult brain had a positive correlation with the *PN* centroid. Two neural stem cell lines derived from fetal human brain also displayed a *PN* phenotype under normal culture conditions. Tissues displaying the *Mes* signature included bone, synovium, smooth muscle, endothelial, and dendritic cells. In addition, a sample of cultured human fetal astrocytes displayed a clear positive association with the *Mes* centroid. Both hematopoietic stem cells isolated from peripheral blood and the highly proliferative cell line Jurkat had a strong association with the *Prolif* centroid. Interestingly, the two neural stem cell lines shifted signature subclass from the *PN* to the *Mes* class in response to treatment and withdrawal of the neurotrophic factor BDNF.

Upon recurrence, tumors tend to shift toward the *Mes* phenotype

To determine if the molecular signatures that define HGG subclasses are a fixed feature of each tumor case or may change after treatment and disease progression, we compared signatures of 26 pairs of matched specimens that represent primary and recurrent astrocytomas from the same patients. The mean change in signature in all primary versus recurrent sample pairs corresponded to a *loss* in similarity to the *PN* centroid of 0.18 ± 0.06 (mean shift in Pearson r ± SEM), a *gain* in similarity to the *Mes* centroid of 0.20 ± 0.09, and very little change in similarity to the *Prolif* centroid (gain of 0.02 ± 0.08). The differences in shifts with respect to *PN* and *Mes* centroids was statistically significant ($p < 0.005$, Student's t test). Eighteen of the 26 matched pairs remained in the same molecular subclass, while eight pairs changed class upon recurrence (Figure 2C). Of these eight pairs, all but one represent shifts into the *Mes* subclass.

Using a pairwise analysis, significance analysis of microarrays (SAM) identified genes upregulated in the recurrent tumors that switched into the *Mes* subclass (Figure 2D). Upregulated genes included YKL40, CD44, and STAT3, genes previously implicated in GBM biology as well as vimentin (VIM), a classic marker of mesenchymal tissues (Eibl et al., 1995; Rahaman et al., 2002; Tanwar et al., 2002). YKL40 is reported to predict radioresistance in human tumors (Pelloski et al., 2005) and to promote

the centroids. **B:** Different sets of normal cells or tissues resemble each of the three centroids. Samples are as follows: fetal brain, adult brain (brain), two neural stem cell lines derived from fetal tissue (NSC1, NSC2), Jurkat, hematopoietic stem cells (HSC), smooth muscle (SmoMusc), endothelial cells (endothel), synovium (synov), and bone. Neural stem cell lines treated by exposure to and withdrawal from the growth factor BDNF are designated NSC1* and NSC2*.
C: Twenty-six pairs of matched primary and recurrent astrocytomas (red, grade IV; blue, grade III) are represented. Each pair of matched specimens is connected by an arrow that is solid and bold for instances of signature class shift.
D: Genes upregulated in cases that shift into *Mes* subclass upon recurrence. FC, fold change.
E: IHC of YKL40 and OLIG2 in matched primary and recurrent tumors from a case that undergoes a shift from *PN* to *Mes* phenotype.

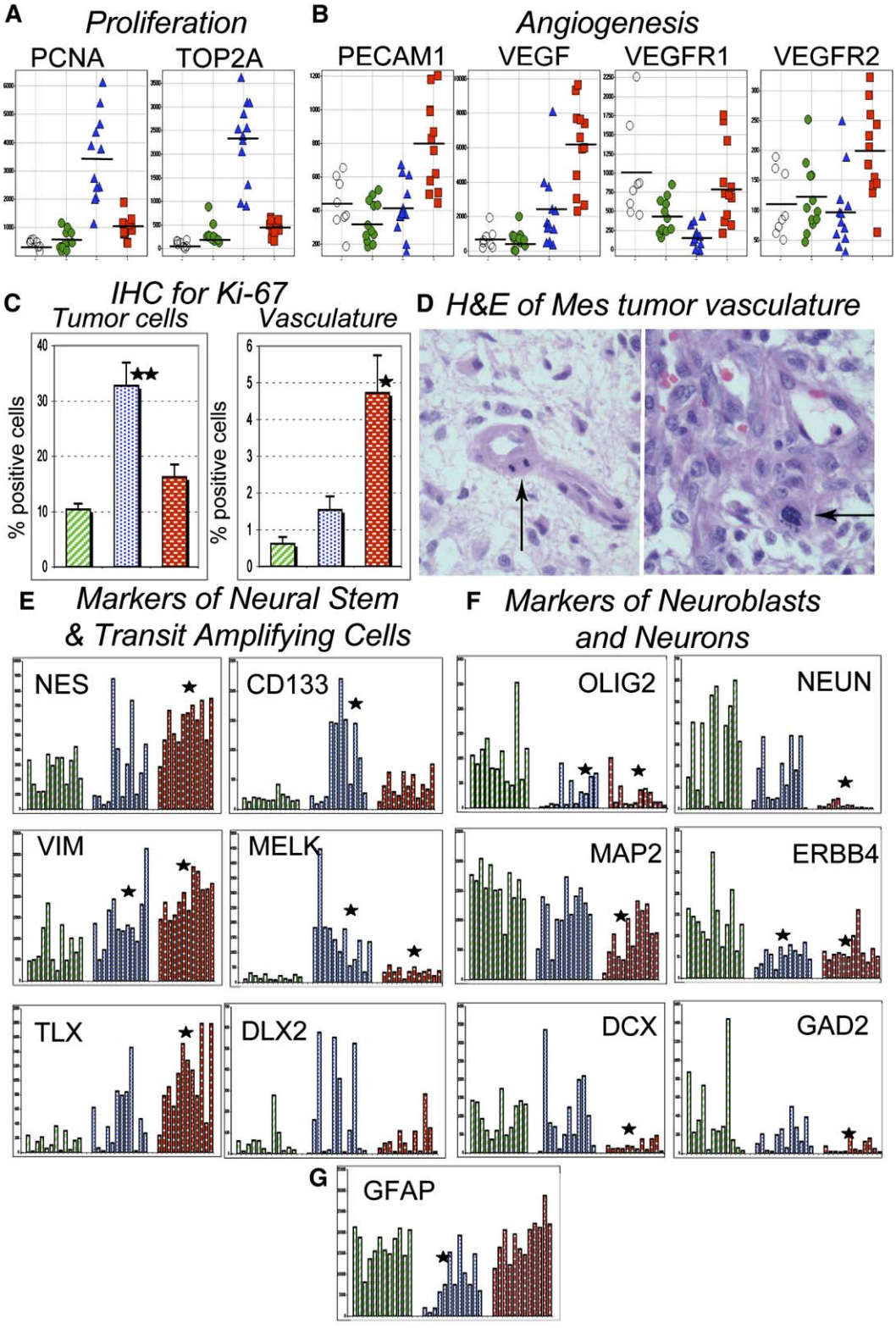

Figure 3. Tumor subclasses are distinguished by markers of proliferation, angiogenesis, and neurogenesis

A and B: Open circles, brain; green circles or bars, *PN*; blue triangles or bars, *Prolif*; red squares or bars, *Mes*. Horizontal bars denote mean values. **A:** *Prolif* HGGs are enriched for expression of PCNA and TOP2A; $p < 1 \times 10^{-6}$ for comparisons with all other groups. **B:** *Mes* HGGs are distinguished by increased expression of PECAM, VEGF, VEGFR1, and VEGFR2; $p < 0.05$ for comparisons with all other groups.

C: Among WHO grade IV tumors, *Prolif* tumors show higher tumor cell Ki-67 labeling index than either *PN* or *Mes* tumors (**$p < 0.002$, both comparisons), while *Mes* tumors show increased Ki-67 labeling index in the vascular cells compared to *PN* or *Prolif* tumors (*$p < 0.01$ both comparisons). Error bars denote standard error of the mean.

clonogenic survival following radiation in vitro (Nigro et al., 2005), findings consistent with a relative increase in expression upon tumor recurrence after treatment. No genes were found to be significantly downregulated in cases that shift into *Mes* class.

Immunohistochemistry (IHC) on tissue from cases that shifted from *PN* to *Mes* upon recurrence suggested frequent loss of OLIG2 expression and upregulation of YKL40 in the recurrent sample. In the example shown in Figure 2E, a *PN* tumor showing prominent nuclear expression of OLIG2, a *PN* marker associated with low-grade lesions (Ligon et al., 2004), exhibited relative loss of OLIG2 expression at recurrence. Normal brain exhibited only low-level staining in oligodendroglia, indicating that upregulation of this marker by *PN* tumors in array data is not a manifestation of normal brain contamination during tissue processing. Conversely, while YKL40, a *Mes* marker, was expressed only in rare tumor cells in the primary sample, abundant expression is seen in the recurrence. Such changes in relative expression of YKL40 were seen in all tumors examined with a *Mes* shift at recurrence.

Poor prognosis tumor subtypes are distinguished by markers of proliferation or angiogenesis

To determine whether proliferation or angiogenesis may contribute to differences in aggressiveness of tumor subclasses, we examined expression of relevant markers in a set of AA/GBMs that included 12 representative cases of each subclass. Proliferating cell nuclear antigen (PCNA) and topoisomerase II α (TOP2A), markers of proliferation, were overexpressed in *Prolif* as compared to *PN* or *Mes* tumors (Figure 3A). *Mes* tumors displayed overexpression of angiogenesis markers, including VEGF, flt1/VEGFR1, kdr/VEGFR2, and the endothelial marker PECAM1 (Figure 3B).

To directly address whether GBM molecular subtypes differ in the extent of tumor cell proliferation and/or microvascular proliferation (MVP), IHC with Ki-67 was employed on a set of clear examples of each molecular subtype of WHO grade IV astrocytoma (Table S1; n = 8 *PN*, 11 *Prolif*, 11 *Mes*). The mean percent of Ki-67-positive tumor cells was higher in *Prolif* tumors compared to the *PN* or *Mes* tumors (Figure 3C). In contrast, Ki-67 index in the vasculature was higher in *Mes* tumors compared to either remaining subtype (Figure 3C). We also noted frequent mitotic figures in the vascular cells of *Mes* tumors (Figure 3D) and their absence in nearly all *Prolif* or *PN* tumors.

Tumors of poor prognosis subtypes express markers of neural stem cell and/or transit-amplifying cells, while tumors of the *PN* subclass express markers of neuroblasts or neurons

Some of the *PN* markers in the signature gene set, such as NCAM, GABBR1 and SNAP91, are associated with neurons. In light of recent findings that tumorigenic cells of GBM express the neural stem cell marker CD133 (Singh et al., 2004), we sought to compare the expression of markers for neural stem cells versus markers of committed neuronal lineage (Figures 3E–3G). We selected markers associated with adult forebrain neurogenesis (Abrous et al., 2005; Anton et al., 2004; Nakano et al., 2005; Shi et al., 2004). For five out of six markers of neural stem cells or multipotent transit-amplifying cells, one or both of the poor prognosis tumor subclasses showed elevated expression compared to *PN* tumors (Figure 3E). Such differences were seen with VIM, nestin (NES), TLX, CD133, and MELK. While DLX2, a marker of transit-amplifying cells, did not show statistically significant differences between tumor groups, some *Prolif* tumors showed strong expression of this gene. In contrast to stem cell markers, markers of neuroblasts or developing neurons were overexpressed in *PN* tumors as compared to *Prolif* and/or *Mes* tumors (Figure 3F). These markers include OLIG2, MAP2, DCX, ENC1 (NeuN), ERBB4, and GAD2. Expression of neuronal markers in *PN* tumors was not accounted for by contamination of tumor specimens with normal brain, as expression levels of OLIG2, DCX, NeuN, and GAD2 were elevated in tumors as compared to normal brain specimens (data not shown; $p < 0.005$ for all Student's t test comparisons of tumor versus normal). GFAP, a marker of both neural stem cells and astrocytes, was more strongly expressed in tumors of both *Mes* and *PN* subclasses as compared to *Prolif* tumors (Figure 3G).

Losses on chr 10 and gains on chr 7 are associated with *Prolif* and *Mes* tumor subtypes

Of the cases examined by expression profiling, DNA from 96 specimens of AA and GBM was available for analysis by array comparative genomic hybridization (CGH). Tumors were scored for relative copy number changes on chrs 1, 7, 10, and 19. The majority of samples demonstrated gains on chr 7 and losses on chr 10, and there were striking differences between tumor subclasses in the frequency of such changes (Figure 4A; $p < 1 \times 10^{-10}$ for chr 10, $p < 1 \times 10^{-6}$ for chr 7, Fisher's exact test). While the majority of *Prolif* and *Mes* tumors had losses on chr 10 that span 10q23.3 (78% and 84%, respectively) and gains on chr 7 (74% and 82%, respectively), a minority of the *PN* tumor subclass showed losses on chr 10 or gains on chr 7 (20% and 23%, respectively). For *Mes* tumors, most cases had relative losses at all loci on chr 10 and gains of all loci on chr 7. In contrast, *Prolif* tumors had more heterogeneous patterns of losses on chr 10. A significant association was also seen between tumor signature and relative copy number changes on chr 19q (Figure 4A; $p < 0.005$), but not on chr 1p or chr 1q ($p > 0.05$).

Given the association between relative genomic copy number changes and tumor subtypes, we sought to determine whether the genes that define each tumor subtype show differences in the distribution of chromosomal locations. Chi-square analysis on the extended lists of tumor subclass markers (Table S3) revealed that, for each of the three lists, the observed frequencies of chr locations differed significantly from that expected by the frequencies of locations for all probe sets on the expression arrays (Figure 4B and Figure S2, $p < 1 \times 10^{-14}$ for *PN*, $p < 0.001$ for *Prolif*, $p < 0.0005$ for *Mes*). *PN* and *Mes* marker lists overrepresent markers on chrs 10 and 19, respectively ($p < 0.05$ for both

D: *Mes* tumors were characterized by the frequent occurrence of mitotic figures (arrows) in the vascular component.
E and F: Relative to *PN* tumors, *Prolif* and/or *Mes* tumors show stronger expression of the neural stem and transit-amplifying markers VIM, NES, TLX, CD133, MELK, and DLX2 (**E**) and weaker expression of the neuroblast and neuronal markers OLIG2, MAP2, DCX, NeuN, ERBB4, and GAD2 (**F**). Asterisk indicates difference from *PN* ($p < 0.05$).
G: GFAP expression is decreased in *Prolif* tumors relative to either *PN* or *MES* tumors.

A

	Chr 10			Chr 7			Chr 19q		
	intact	loss 10q23.31	loss	no gain	partial gain	gain	loss	no change	gain
PN	28	5	2	27	3	5	6	28	1
Prolif	5	6	12	6	3	14	3	15	5
Mes	6	2	30	7	4	27	1	24	13

B

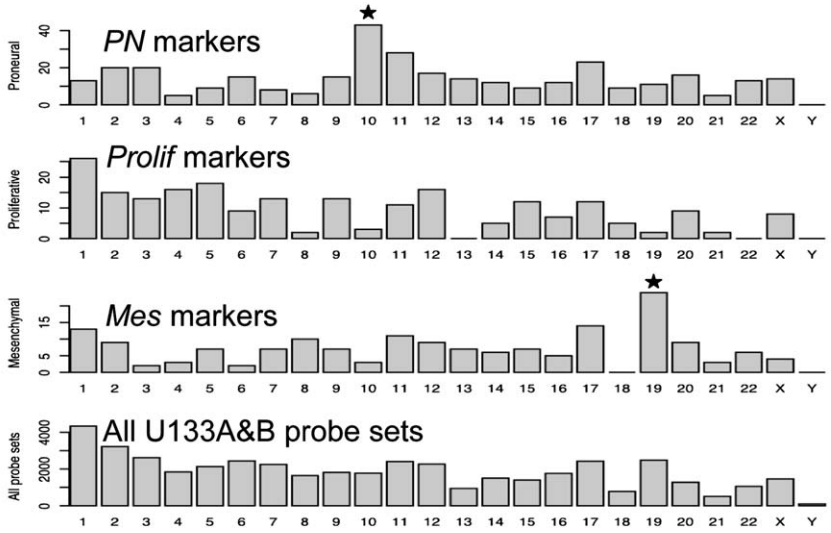

Figure 4. Copy number changes on chrs 7, 10, and 19 differ in tumor subclasses and are reflected in expression signatures

A: Frequencies of copy number changes of chrs 10, 7, and 19q as a function of tumor signature subclass. For chr 10, tumors are reported as exhibiting either no losses, losses confined to 10q that include the *PTEN* locus, or losses of essentially all loci. For chr 7, cases are scored as no gains, gains of any portion of chr 7, or gain of all loci. For chr 19q, cases are scored as gains or losses if over one-half of the loci show copy number changes.

B: Number of probes sets in *PN*, *Prolif*, or *Mes* tumor marker lists (as labeled) compared to all U133A and U133B probe sets plotted as a function of chromosome location.

comparisons after Bonferroni correction for 72 comparisons). These findings corroborate the differences between tumor subtypes in relative DNA copy number changes on chrs 10 and 19q.

Markers of Notch and Akt pathways are differentially expressed in tumor subclasses with good versus poor prognosis

Consistent with the association of chr 10 loss and tumor subclass, examination of array CGH data for the *PTEN* locus confirmed that a high percentage of *Prolif* and *Mes* cases displayed relative losses of this locus. A negative association was seen between CGH ratios for the *PTEN* locus and similarity to the *PN* centroid (Figure 5A). Most cases of gains or amplifications of the *EGFR* locus were tumors of either *Prolif* or *Mes* subclasses, and a negative correlation was seen between *EGFR* copy number gains and similarity to the *PN* centroid (Figure 5B). No obvious amplifications or deletions were seen at loci corresponding to *AKT1*, *AKT2*, or *AKT3*, nor of catalytic subunits of PI3K (data not shown). A small number of samples demonstrated relative copy number gain for *PIK3R3*, a regulatory subunit of PI3K, and CGH ratios for this locus were positively correlated with similarity to the *Prolif* signature (Figure 5C).

Since our results suggested strong relationships between Akt pathway activation and tumor subtypes, we compared PTEN mRNA expression and phospho-Akt (p-Akt) IHC in tumor subtypes. We found that *Prolif* and *Mes* tumors expressed approximately 2-fold lower PTEN mRNA and stronger p-Akt (ser473) as compared to *PN* tumors (Figures 5D and 5I). The results were highly significant ($p < 5 \times 10^{-5}$ for PTEN mRNA, $p < 5 \times 10^{-8}$ for p-Akt IHC for Student's t tests of *PN* versus other). The PTEN results were validated in a second independent sample set (Tables S1 and S5).

When we examined the complete list of *PN* tumor markers in the MDA sample set (Table S3), probe sets corresponding to the Notch pathway elements DLL3, DLL1, HEY2, and ASCL1 met our criteria for markers of *PN* tumors (Figures 5E–5H). These genes were confirmed to be overexpressed in *PN* tumors of the validation data set (Table S5). Each of these Notch pathway elements has been implicated in forebrain neurogenesis (Campos et al., 2001; Casarosa et al., 1999; Sakamoto et al., 2003), and ASCL1 has recently been linked to specification of both neurons and oligodendroglia in the adult forebrain (Parras et al., 2004). Elements of the Notch pathway for which microarray data did not show upregulation in *PN* tumors include NOTCH1–NOTCH4, JAG1 and JAG2, HES1, HES2, HES4, HES6, and HES7 (data not shown). HEY1 showed a small but significant upregulation in MDA *PN* tumors (1.4 fold change, $p = 5 \times 10^{-5}$).

To examine direct evidence for Notch signaling activation, we utilized a blinded assessment of nuclear Notch immunoreactivity in all MDA cases with available paraffin-embedded sections. Positive cases showed a weak but discernible "blush" in the nucleus, as compared to negative cases, which showed a complete absence of nuclear staining. Figure 5J displays frequencies of each tumor subtype rated 0, 1, or 2 for Notch nuclear staining. Ratings of *PN* samples were demonstrated to be significantly higher than those of either *Prolif* ($p < 0.005$, Student's t test) or *Mes* ($p < 0.001$, Student's t test) subclasses.

A two-gene model of DLL3 and PTEN expression predicts survival of high-grade astrocytoma

Since our data suggested a role for Notch and Akt pathways in tumor aggressiveness, we sought evidence for a direct association between expression of pathway markers and survival.

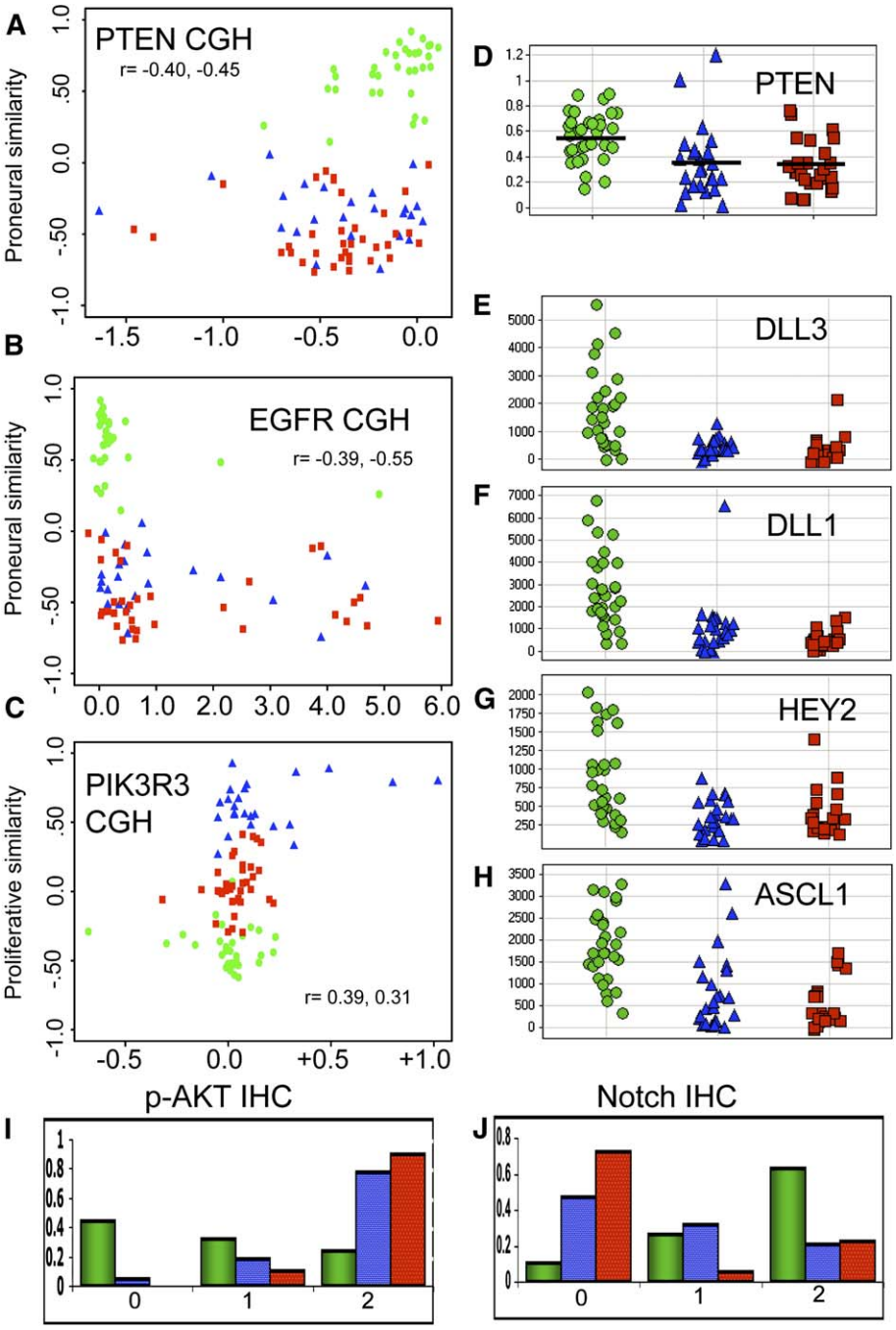

Figure 5. *Prolif* and *Mes* tumors display differential activation of Akt and Notch pathways

PN, *Prolif*, and *Mes* tumors are denoted by green circles, blue triangles, and red squares, respectively.

A–C: For each sample, the x axis displays the CGH log2 ratio for the locus sampled, while the y axis indicates similarity to either the *PN* or *Prolif* centroid, as indicated. r values indicate Pearson and Spearman correlation coefficients between CGH ratios and centroid similarities. *PTEN* loss (**A**) and *EGFR* amplification (**B**) are negatively associated with the *PN* signature, while gain of the *PIK3R3* locus (**C**) is positively associated with the *Prolif* signature.

D: Normalized PTEN mRNA levels are lower in poor prognosis tumor subtypes compared to the *PN* tumor subclass. Horizontal lines denote group means.

E–H: *PN* tumors show strong overexpression of the Notch pathway elements DLL3, DLL1, HEY2, and ASCL1.

I and J: Tumor subclasses differ in staining for p-Akt and nuclear Notch. For each tumor subtype, the fraction of samples rated as 0, 1, or 2 for p-Akt (**I**) or nuclear Notch (**J**) immunostaining is depicted. *PN*, *Prolif*, and *Mes* subtypes are indicated by green, blue, and red bars, respectively.

For this analysis, we evaluated PTEN mRNA by qPCR and DLL3 mRNA by microarray data from all samples in the MDA survival set where sufficient mRNA was available (n = 65). A Cox model revealed that levels of PTEN and DLL3 mRNA and their statistical interaction were all associated with survival in high-grade astrocytoma and combined to form a highly significant predictive model (likelihood ratio test of 21.6 compared to a chi-square reference distribution with 3 degrees of freedom; $p < 0.0001$). The predicted survival functions depicted in Figure 6A demonstrate that low expression of PTEN mRNA was associated with poor survival regardless of the level of DLL3 expression. For the circumstance of high PTEN expression, estimated survival varied as a function of DLL3 such that high levels of both PTEN and DLL3 mRNAs were associated with the best outcome. We next fitted the same model with a smaller (n = 34) independent set of UCSF grade III and IV astrocytomas and found that the resulting predicted survival curves were strikingly similar to those obtained from the MDA sample set (Figure 6B).

Expression signatures of GBM cell lines predict EGF/FGF-independent neurosphere growth

To examine the biological significance of the molecular tumor signatures, we examined the ability of GBM cell lines with varying signatures to grow neurospheres. We profiled 16 GBM cell lines for mRNA expression and investigated their ability to generate neurospheres in the presence or absence of EGF + FGF.

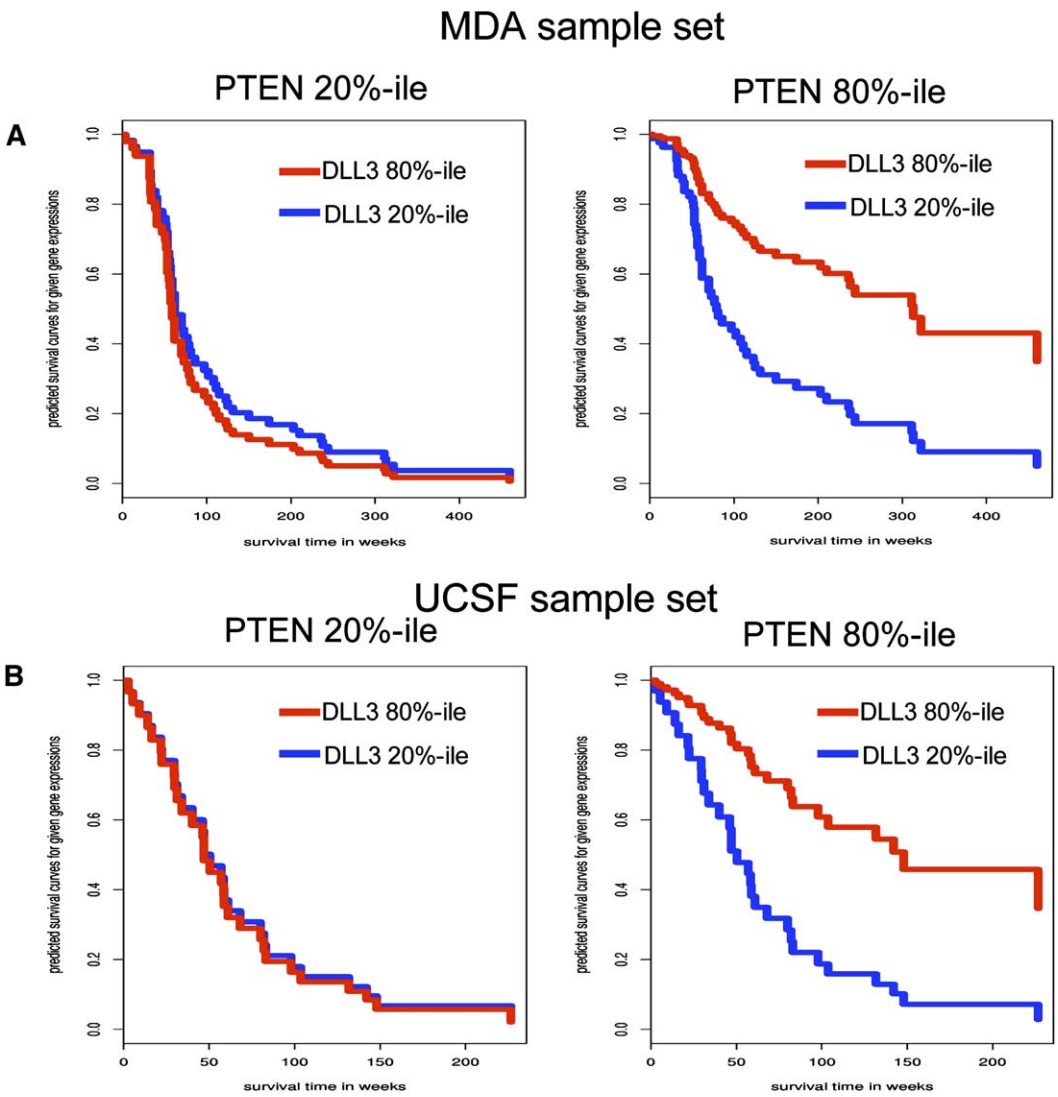

Figure 6. Expression of PTEN and DLL3 predicts survival of high-grade astrocytoma

A and B: Estimated survival functions of two sample populations (n = 76 for **A**; n = 34 for **B**) modeled for the instance of PTEN expression at the 20th (left) and 80th percentile (%-ile, right). Blue and red lines show estimated survival for samples with DLL3 expression at the 20th and 80th %-ile of expression, respectively.

All 16 lines were negatively correlated with respect to the *PN* centroid but showed a wide range of similarities to the *Mes* and *Prolif* centroids. While 15 of the 16 cell lines generated neurospheres that could be propagated in EGF + FGF, their ability to generate neurospheres that grow in the absence of EGF + FGF varied (Figure 7A) and was correlated with the expression signature of the parental cell line (Figure 7B). Most strikingly, we found that the two cells lines most negatively correlated to the *Mes* centroid (G112 and G122) generated neurospheres that grew rapidly in the absence of EGF + FGF, while cell lines with a strong positive correlation to the *Mes* centroid failed to generate neurospheres that could be readily propagated in the absence of EGF + FGF (Figure 7B).

Summary of findings

A summary of major findings, including the parallels between tumor subtypes and stages in forebrain neural development, is displayed in Figures 8A and 8B.

Discussion

At present, gliomas are diagnosed by histopathological criteria, and known robust prognostic factors for most of these tumors are limited to tumor grade and patient age. The widespread acceptance that losses on chrs 1p and 19q are of prognostic value in oligodendroglioma (Cairncross et al., 1998) has spurred interest in developing molecular markers to predict outcome and response to treatment across a broader population of gliomas. While numerous genetic alterations have been described in GBM (von Deimling et al., 1995; Watanabe et al., 1996), such markers have proved to be of marginal utility in predicting outcome or guiding decisions about disease management. Importantly, recent expression profiling studies have revealed that molecular classification of gliomas can be of prognostic value (Freije et al., 2004; Nutt et al., 2003). In the current study, we identify molecular signatures associated with tumor aggressiveness as well as with disease progression and relate these signatures to differences in signaling pathways implicated in gliomagenesis.

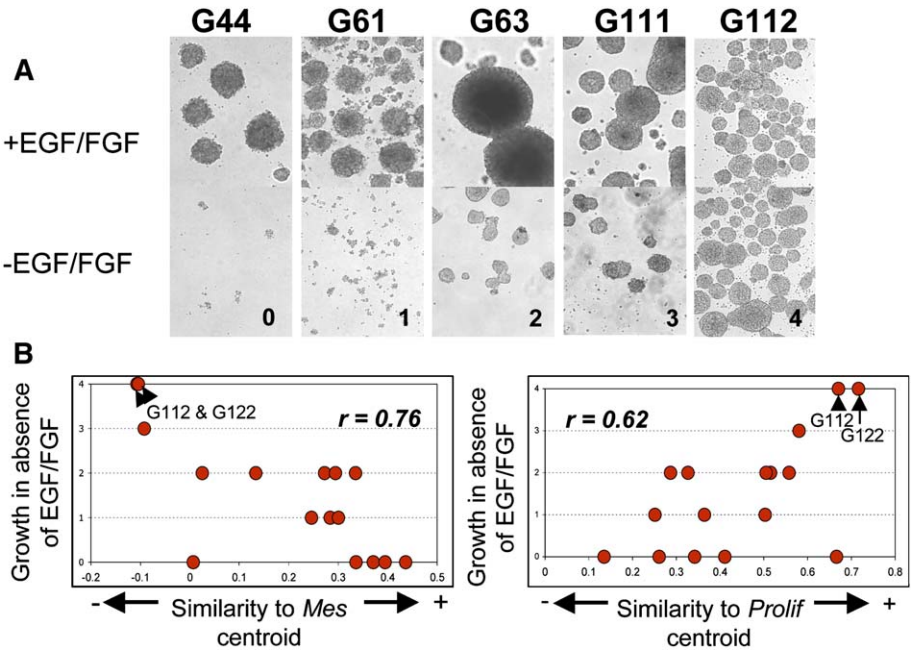

Figure 7. Expression signatures of glioma cell lines predict neurosphere growth

A: Neurosphere cell line cultures (names as indicated) maintained in the presence or absence of EGF + FGF, showing range of growth (rated 0–4) in the absence of EGF + FGF.

B: Neurosphere growth of 16 cell lines as a function of correlation of expression signature to the *Mes* or *Prolif* centroids. Spearman r as indicated.

Tumor subclasses have prognostic value and delineate a pattern of disease progression

We report here a previously unreported prognostic classification scheme for HGG that assigns tumors to subtypes based on similarity to defined expression signatures. This classification scheme offers prognostic value that is independent of tumor grade and that may be useful for predicting outcome of GBM cases. Each of the three molecular subtypes of glioma identified resembles a distinct set of tissues and is enriched for markers of different aspects of tissue growth. While the current analysis utilizes a set of 35 signature genes, these molecules are representative of much longer lists of markers that identify each tumor subtype. One HGG subtype, which we term proneural (*PN*), is distinguished by markedly better prognosis and expresses genes associated with normal brain and the process of neurogenesis. Two poor prognosis subtypes, characterized by a resemblance to either highly proliferative cell lines or tissues of mesenchymal origin, show activation of gene expression programs indicative of cell proliferation or angiogenesis, respectively. We speculate that the poor survival associated with the *Prolif* and *Mes* tumor types is related to a growth advantage conferred by either a rapid rate of cell division or enhanced survival of tumor cells afforded by neovascularization. Quantitative assessment of Ki-67 IHC in a set of WHO grade IV astrocytomas revealed that *Prolif* tumors exhibit a higher percentage of cycling tumor cells compared with other subclasses, while *Mes* tumors exhibit evidence of increased MVP. Previous studies have suggested the prognostic value of markers of proliferation or angiogenesis in glioma (Ho et al., 2003; Hsu et al., 1996; Osada et al., 2004) but have not indicated the existence of distinct GBM subsets that are differentially associated with these processes. Of note, our *Prolif* and *Mes* glioma subtypes are characterized by expression of portions of a wound-healing signature that has been associated with poor outcome in several epithelial tumor types (Chang et al., 2005).

We note that grade III tumors and grade IV tumors lacking necrosis were predominately *PN* subtype. Importantly, however, the *PN* tumor subtype also includes a set of GBM tumors with improved outcome that display necrosis and cannot be distinguished from poor prognosis tumor subtypes by qualitative histological examination. Thus, our results add to the growing consensus that molecular categorization may prove to be superior to histological grading in predicting prognosis.

The tumor subtypes identified in the current study bear resemblance to previously reported prognostic subtypes identified by expression profiling. In particular, three previous studies report phenotypes that closely resemble the *PN* and *Mes* HGG subtypes that we describe (Freije et al., 2004; Liang et al., 2005; Nigro et al., 2005). In addition, previous work (Godard et al., 2003) highlights a cluster of angiogenic genes defining a tumor subpopulation that appears similar to our *Mes* tumor subtype. Our observation of a mutually exclusive pattern of expression of *PN* versus *Mes* markers helps explain the consensus regarding the existence of these two tumor subtypes. Even within tumor specimens that express both *PN* and *Mes* markers, the spatial distribution appears to be nonoverlapping. The strong association between loss of chr 10 and the *Mes* signature is consistent with previous findings linking chr 10 loss to prognostic tumor subtypes (Nigro et al., 2005) and with the demonstration of antiangiogenic actions of chr 10 introduction into GBM cell lines (Hsu et al., 1996).

The existence of a distinct tumor subtype that is enriched for proliferative markers has been noted by one previous report (Freije et al., 2004) but not described in other studies. Our findings indicate that the *Prolif* signature is less exclusive than *PN* or *Mes* signatures and that the proportion of gliomas that occur with a *Prolif* signature varies across sample populations obtained from different institutions. In support of our categorization of the *Prolif* tumor subclass as a distinct molecular subtype of tumor, we point to the existence in *Prolif* tumors of a pattern of genomic alterations that distinguishes this tumor subtype. Most notably, gains of the *PIK3R3* locus on chr 1 appear to be a feature that is unique to tumors of the *Prolif* class. The existence of a genomic alteration unique to tumors bearing the *Prolif*

A

	Proneural	Proliferative	Mesenchymal
Histological grade	WHO grade III or WHO grade IV with or without necrosis	WHO grade IV with necrosis	WHO grade IV with necrosis
Cellular morphology	Astrocytic or Oligodendroglial	Astrocytic	Astrocytic
Evolution of signature	Arises in 1° tumor, may persist or convert to *Mes*	Arises in 1° tumor, may persist or convert to *Mes*	Arises in 1° tumor or by conversion from other subtype
Patient age	Younger (~40 yrs.)	Older (~50 yrs.)	Older (~50 yrs.)
Prognosis	Longer survival	Short survival	Short survival
Histological Markers	Olig2, DLL3, BCAN	PCNA, TOP2A	CHI3L1/YKL40, CD44, VEGF
Tissue similarities	Adult and Fetal Brain	HSC, lymphoblast	Bone, cartilage, smooth musc, endothelium, dendritic cells
Biological process	Neurogenesis	Proliferation	Angiogenesis
Analogous forebrain cell	Neuroblast	Neural Stem Cell and/or Transit Amplifying Cell	Neural Stem Cell
Chromosome gain/loss	None	Gain of 7 & Loss of 10 or 10q	Gain of 7 & Loss of 10
PTEN locus	PTEN intact	PTEN loss	PTEN loss
EGFR locus	EGFR normal	EGFR amplified or normal	EGFR amplified or normal
Signaling	Notch activation	Akt activation	Akt activation

B

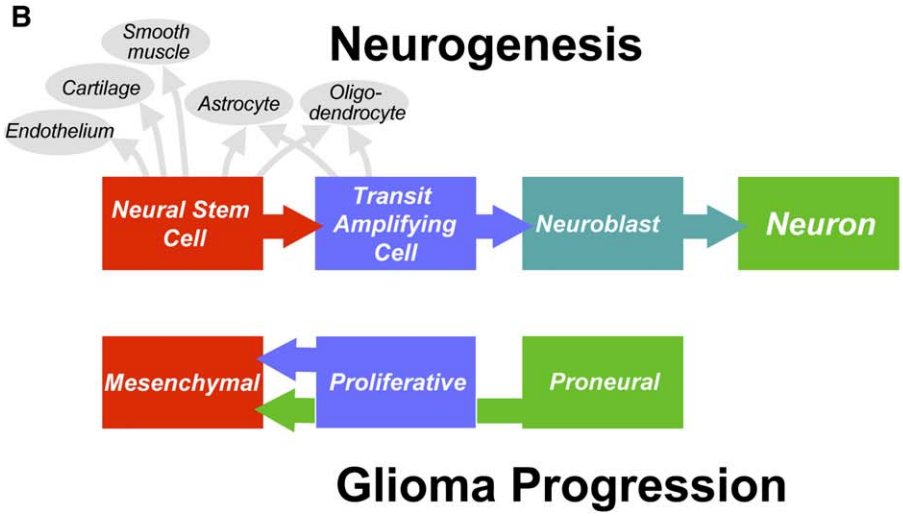

Figure 8. Summary of tumor subtypes

A: Major features of tumor subtypes.

B: Model depicting parallels between tumor subtypes and stages in neurogenesis.

signature argues in favor of the designation of these tumors as a distinct subclass and suggests that epidemiological factors may have influenced the incidence of this subclass in the populations we investigated.

The striking mutual exclusivity of the *PN* and *Mes* tumor signatures suggests the possibility that these tumor subtypes reflect distinct disease entities, perhaps arising from different cell types of origin. By studying matched pairs of primary and recurrent tumors from the same patients, however, we observe that some tumors that originally arise as *PN* or *Prolif* subtype recur with a *Mes* signature. Focal expression of YKL40, a marker of the *Mes* phenotype, is seen in primary tumors, including those that shift to *Mes* class upon recurrence. Notably, no instances are seen of tumors gaining appreciable *PN* character between initial presentation and recurrence. Taken together with the ability of neural stem cell lines to shift from *PN* to *Mes* signature, the ability of tumors to change subclass suggests that the tumor subtypes may represent alternate differentiation states of disease. We cannot, however, rule out the possibility that some apparent shifts may reflect tumor heterogeneity rather than temporal changes in tumor character. In addition, our experimental design does not allow us to distinguish between alterations in gene expression that reflect disease progression from those which are elicited by treatment. Nevertheless, our finding of

unidirectional subclass shifts suggests the possibility that tumor cells can acquire the *Mes* phenotype through accumulation of genetic or epigenetic abnormalities. The older age of patients with *Mes* subtype tumors is consistent with this hypothesis.

While we have no direct evidence for molecular events that underlie the apparent shift in tumor cell signature, the strong correlation between losses of chr 10 and the *Mes* signature may offer an important insight into the biology of disease progression. Regardless of underlying mechanism, shifts toward the *Mes* phenotype appear to be a common pattern of disease progression and are reminiscent of epithelial-to-mesenchymal transitions that are associated with increased malignant behavior of epithelial tumor types.

Markers in Notch and Akt pathways predict glioma aggressiveness

Our findings demonstrate evidence at genomic, mRNA, and protein levels for activating alterations of Akt signaling in tumors of poor prognosis subtypes. A wealth of previous data support a role for Akt signaling in promoting the formation and growth of high-grade glial malignancies (Knobbe et al., 2002; Sonoda et al., 2001). A series of elegant studies in genetically engineered mouse models has convincingly demonstrated a role for Akt in promoting formation and growth of glial malignancies (Holland et al., 2000; Rajasekhar et al., 2003; Uhrbom et al., 2002; Xiao et al., 2005). In human tumors, both *EGFR* amplification and *PTEN* deletion are well-known alterations that activate Akt and are specifically associated with the distinction between GBM versus lower-grade lesions (Stiles et al., 2002). More recently, both mutations in *PIK3CA* and balanced copy number increases in *PIK3CA* and *PIK3CD* have been described in AA and GBM (Broderick et al., 2004; Mizoguchi et al., 2004; Samuels et al., 2004). While the prognostic value of *EGFR* amplification or genetic changes in PI3K subunits is not clear, several studies have shown that losses on chr 10, loss of the *PTEN* locus, or enhanced PI3K signaling are all associated with poor outcome in GBM (Chakravarti et al., 2004; Lin et al., 1998; Schmidt et al., 2002; Tada et al., 2001). Activation of PI3K/Akt signaling is implicated in several biological processes that confer a growth advantage, including proliferation, survival, and angiogenesis (Abe et al., 2003; Pore et al., 2003; Su et al., 2003). Thus, we speculate that the poor outcome of *Prolif* and *Mes* subtype tumors may result, in part, from actions of PI3K/Akt signaling to promote more aggressive growth patterns characterized by high rate of proliferation or neoangiogenesis, respectively. Current findings do not lend a clear hypothesis to explain the divergence between the proliferative versus angiogenic manifestations of Akt signaling in the two poor prognosis subtypes, but one possibility is that more frequent loss of loci on chr 10p or gains on chrs 7 and 19q in *Mes* tumors may contribute to this distinction. The high frequency of *Mes* markers encoded for on chr 19 is interesting in this regard.

Activation of NOTCH1 signaling has been recently linked to several malignancies, including glioma (Fan et al., 2004; Purow et al., 2005; Radtke and Clevers, 2005; Weng et al., 2004). Our observations demonstrate prognostic value of Notch pathway markers in HGGs. Specifically, NOTCH1 nuclear staining and mRNA for several Notch pathway elements are enriched in the better outcome *PN* tumor subtype as compared to poor prognosis subtypes. Further, we find in two independent sample populations that expression of mRNA for DLL3 is correlated with longer survival, particularly in cases where PTEN expression is high. While several interpretations are possible, one interesting possibility is that in the presence of intact PTEN, inhibitory activity of DLL3 on Notch signaling (Ladi et al., 2005) may limit tumor growth by promoting a more differentiated phenotype. Regardless of the precise role of Notch signaling, the prognostic value of our two-gene PTEN and DLL3 Cox model clearly suggests Akt and Notch signaling as major determinants of tumor growth.

Parallels between regulation of glioma growth and forebrain neurogenesis

The current investigation links prognostic tumor subtypes to differences in relative expression of neural stem cell versus neuroblast markers as well as to differences in Akt and Notch signaling elements. One model for human gliomas is that all molecularly defined subtypes arise from similar cell type(s) of origin, but some tumors are maintained in more undifferentiated neural stem cell-like (*Mes*) or transit-amplifying-like (*Prolif*) phenotypes, while others (*PN*) adopt a phenotype closer to that of neuroblasts or immature neurons. This model, supported by animal studies (Bachoo et al., 2002; Fomchenko and Holland, 2005), suggests that HGGs may arise from cells at multiple stages of differentiation from stem cell to neuron or glia, and that phenotypic variations among HGGs are determined in large part by molecular alterations in signaling pathways rather than by differences in cell type of origin. In light of the critical roles that PTEN and Notch exert during forebrain neurogenesis to maintain neural stem cells or progenitors in a proliferating undifferentiated state (Groszer et al., 2001; Sakamoto et al., 2003; Yoon and Gaiano, 2005), our findings suggest that aggressiveness of glioma growth may be largely governed by processes that regulate cell fate choices during neurogenesis.

The phenotype of the tumor subtypes described in this study parallels stages in neurogenesis in the adult forebrain (Figure 8). Similar to committed neuronal precursors, tumors of the *PN* subtype appear to have a low rate of proliferation and express markers seen on neuroblasts and immature neurons. In contrast, *Mes* and *Prolif* subtype tumors lack neuronal lineage markers but recapitulate aspects of neural stem cells and/or transit-amplifying cells. The parallel between the apparently rapid rate of proliferation of *Prolif* tumors and the transit-amplifying cells is readily apparent. In addition, we find that tumors of the *Prolif* subtype are characterized by robust expression of MELK, a marker of rapidly proliferating multipotential precursor cells in the rodent forebrain (Nakano et al., 2005). Further, the *EGFR* amplifications in tumors of both *Prolif* and *Mes* subclasses parallel the responsiveness of both neural stem cells and transit-amplifying cells to EGF (Doetsch et al., 2002). The expression of smooth muscle, endothelial cell, and cartilage markers by *Mes* tumors is reminiscent of the reported multipotentiality of neural stem cells from adult forebrain (Bani-Yaghoub et al., 2004; Rietze et al., 2001; Sieber-Blum, 2003; Wurmser et al., 2004). One caveat in interpretation, however, pertains to the possibility that tumor expression profiles may be confounded by recruitment of stem cell-like populations to the tumor mass.

Intriguingly, the parallels between the *Mes* tumor phenotype and neural stem cells include a recapitulation of the close association seen between neural stem cells and endothelial cells. In contrast to other tumor subtypes, *Mes* tumors display robust expression of VEGF, its receptors, and markers of endothelial

cells. Recent findings indicate that VEGF promotes proliferation and survival of adult forebrain neural stem cells and demonstrate that secreted factors from endothelial cells also promote neural stem cell proliferation (Cao et al., 2004; Fabel et al., 2003; Jin et al., 2002; Maurer et al., 2003; Schanzer et al., 2004; Shen et al., 2004; Yasuhara et al., 2004; Zhu et al., 2003). It is interesting to speculate that the growth of tumor cells of *Mes* phenotype tumors may be supported by the actions of increased levels of VEGF and/or endothelial-derived factors. In this regard, therapies that target VEGF or its receptors might prove beneficial in not only targeting neovasculature, but also directly inhibiting growth of tumor cells that manifest a neural stem cell-like biology. Targeted inactivation of *VEGF* in the neural tube has been recently demonstrated to produce both vascular defects and a profound degree of neuronal apoptosis in the murine forebrain (Raab et al., 2004).

Our in vitro finding that neurosphere growth of GBM cell lines correlates with expression signature suggests that the stem cell-like behavior of primary tumors might also be predicted from signature subclass. These findings point to the possibility that expression signatures may predict responses of both cell lines and primary tumors to targeted therapies.

Therapeutic implications

The present findings offer several implications for the development of effective therapies for glioma. First, the current investigation adds to the growing consensus that optimal treatment of glial malignancies may rely on regimens targeted at distinct molecular categories of tumor (Mischel et al., 2003; Newton, 2004; Rao et al., 2003). Second, our findings support the value of targeting both Akt and Notch pathways in the potential development of novel therapeutic regimens for HGG. Third, the suggestion that tumor recurrence after standard therapies may be accompanied by a phenotypic shift into a mesenchymal, angiogenic state underscores the value of targeting this aggressive phenotypic state even in tumors with a less aggressive phenotype. Finally, correlations between stem cell biology and glioma aggressiveness suggest that greater understanding of forebrain neurogenesis may lead to novel insights for therapeutic intervention in glial malignancies.

Experimental procedures

Tumor samples and patient characteristics

A summary of all glioma cases studied is included in Table S1. For survival analysis, two expression profiling data sets were generated using frozen tissue samples from 76 MDA cases and RNA from 39 UCSF cases (Nigro et al., 2005). Cases analyzed met the following criteria. Fresh-frozen samples were obtained at the time of initial surgical resection from patients (>21 years of age) without prior therapy. Clinical follow-up information was available for a period of at least 2 years postsurgery or until death. Institutional Review Board/Human Subjects approval was obtained for these retrospective laboratory studies at UCSF and MDA. Cases were graded according to WHO criteria (Kleihues and Cavenee, 2000; see Table S2), and sections from frozen tissues were examined by a neuropathologist (K.A.) to ensure that $\geq$90% of the sample represented tumor. Unusual histological variants were excluded. In addition, a third previously published data set study (Freije et al., 2004) was utilized for validation of the prognostic value of our classification scheme. For analysis of this data set (Figure S1), we utilized data from all cases that met our criteria for patient age and microarray quality control parameters, including cases of oligodendroglial or mixed morphology as well as cases with survival times censored at less than 2 years.

Normal adult brain tissue consists of autopsy specimens of cerebral cortex from donors with no history of brain tumor or neurological disorders and was obtained from the National Neurological Research Brain Bank (Los Angeles, CA). Description of samples analyzed in Figure 2B, some of which were profiled at GeneLogic Inc (Gaithersburg, MD), is included in Table S4.

Gene expression profiling, CGH, and qPCR

For glioma and brain specimens not included in previous publications (Freije et al., 2004; Nigro et al., 2005), total cellular RNA was extracted using Qiagen's RNA isolation kit according to the manufacturer's protocol. Genomic DNA contamination was removed through an on-column DNase digestion step. Affymetrix U133A and U133B chips were employed for expression profiling according to a previously published technique (Tumor Analysis Best Practices Working Group, 2004). Quality control parameters were as described in this publication with the exception that 3′/5′ ratios of >3 for actin were allowed if the 3′/5′ ratio for GAPDH was <3. qPCR was performed in duplicate for each sample on the ABI Prism7700 Sequence Detector (Applied Biosystems, Foster City, CA) with TaqMan PCR Core reagents (Applied Biosystems, Foster City, CA). Twenty-five nanograms of total RNA was used in each 50 μl reaction. RAB14 was used for normalization, as it exhibits very little variation in expression across a large number of samples. All primer pairs were designed to generate amplicons of 67–79 bp. DNA extraction and array CGH were performed as previously described (Misra et al., 2005). Of the 96 samples analyzed via CGH, data for 43 samples came from a previously published study (Nigro et al., 2005). The microarray data have been submitted to Gene Expression Omnibus (GEO), and the accession number for the data series is GSE4271.

Analysis of microarray data

Signal intensity values from Microarray Analysis Suite version 5 were utilized with a scaling factor of 500 for all analysis of microarray data. K-means clustering and agglomerative clustering were performed with the use of Spotfire Decision Site software version 7.3 using Pearson correlation as the similarity measure. For each gene, data were normalized into Z scores prior to clustering. The 35 signature genes used for tumor classification represent the most robust markers for each of three tumor subsets in the MDA survival sample set. Markers of each subset were identified as follows. Each of the 76 samples was assigned to one of three groups by k-means clustering using expression of the 108 genes most strongly correlated with survival. Using a p value cutoff of 1×10^{-4}, Student's t tests were utilized to identify all genes whose expression differed between samples in each subclass compared to tumors of other subclasses. Genes meeting this statistical cutoff and showing at least 2-fold overexpression are included in the extended list of markers for each tumor subset (Table S3). Probe sets used as signature genes for each tumor subtype were determined as follows. For each Student's t test comparison, we rank-ordered the 500 probe sets with the smallest p values by fold change and selected those corresponding to identified full-length sequences that showed the greatest fold change and that met a minimum expression cutoff (mean intensity of 400 within group of interest). Empirical determinations using k-means clustering revealed that stable sample clusters resulted when clustering was performed using 30 to 60 probe sets, provided that the gene list for clustering was balanced to include fewer *Prolif* markers. The final 35 signature genes contained 15 *PN*, 15 *Mes*, and 5 *Prolif* markers. Similarity scores to *PN*, *Prolif*, and *Mes* centroids represent Pearson correlation coefficients to each of the centroids generated in k-means clustering of the 76 MDA survival samples. For statistical comparisons of data presented in Figures 3 and 5, data (or log-transformed microarray data) were analyzed via ANOVA and post hoc Student's t tests with Bonferroni correction. Log-transformed expression data were also utilized for the statistical analysis performed for Figure 6.

In situ hybridization and IHC

^{33}P-UTP-labeled antisense riboprobes were transcribed using in vitro transcription (Promega, Madison, WI) and hybridized to paraffin-embedded human glioma tissue microarrays utilizing a previously described method (Phillips et al., 1990). Images depicted in Figure 1 are from a tissue microarray obtained from Petagen, Inc. The probe to BCAN represents a 668 bp fragment (939 to 1606), and that for YKL40 represents a 1158 bp fragment (121 to 1278).

IHC was performed on paraffin-embedded sections as previously described (Simmons et al., 2001). Primary antibodies were anti-p-Akt (ser473) from Cell Signaling Technology (Beverly, MA), anti-Ki-67 (MIB-1) from Dako

(Carpinteria, CA), anti-Olig2 from Immuno-Biological Laboratories (Fujioka, Japan), and anti-Notch from Santa Cruz Biotechnology (Santa Cruz, CA). Ratings were performed by a neuropathologist (K.A.) blinded to the signature group of the specimens. Ki-67 labeling index in the tumor cells was performed by identifying the highest area of staining on low power, then counting 1000 cells in that region to determine the percent of labeled cells. Proliferation in vascular cells was determined by identifying a positively stained vascular cell (if present) and then counting after randomly choosing additional areas until 100 vascular cells were counted.

In vitro studies

Previously described GBM cell lines were utilized for in vitro studies (Hartmann et al., 1999). For neurosphere cultures, cells positively sorted with CD133 beads were maintained in culture as described for primary GBM specimens (Singh et al., 2004). All neurosphere cultures were maintained in neurobasal medium (Invitrogen) with N2 supplement (Invitrogen) and NSF1 (Cambrex). When present, EGF and FGF were added at a concentration of 20 ng/ml. Each cell line is rated for neurosphere growth in the absence of EGF + FGF by an observer blinded to the molecular signature of the cell lines. Rating scale was as follows: 0 = no viable neurospheres; 1 = slowly expanding neurospheres; 2 = moderate growth rate; 3 = moderate to fast growth, but slower than that seen with EGF + FGF; 4 = rapid growth that is not accelerated by EGF + FGF.

Supplemental data

The Supplemental Data include two supplemental figures and six supplemental tables and can be found with this article online at http://www.cancercell.org/cgi/content/full/9/3/157/DC1/.

Acknowledgments

We thank Keith Black and Julia Ljubimova of Cedars-Sinai Hospital for providing glioma specimens, Wallace Tourtelotte of the National Neurological Research Bank for autopsy specimens of brain, and David Eberhard for confirmation of histopathology of some specimens. Alicia Ledoux, Helen Yang, and Paula Colman assisted with tissue processing for microarray and immunohistochemical studies as well as imaging of histology. GBM cell lines were a generous gift from Manfred Westphal of the University of Hamburg. We extend thanks to Tom Januario, Zemin Zhang, Yan Zhang, Cynthia Honchell, Mike Ward, Alex Abbas, and Jim Fitzgerald for assistance with bioinformatics databases and analysis tools; to AyLy Ling-Tucker for advice on TaqMan-PCR; to Eric Stoelting and Allison Bruce for graphics; and to Susan Palmieri for assistance with photomicroscopy. H.S.P., S.K., R.C., W.F.F., R.H.S., T.D.W., L.S., and Z.M. are full-time employees of Genentech, Inc. K.A. was supported by an institutional research grant from MDACC.

Received: October 6, 2005
Revised: December 2, 2005
Accepted: February 20, 2006
Published: March 13, 2006

References

Abe, T., Terada, K., Wakimoto, H., Inoue, R., Tyminski, E., Bookstein, R., Basilion, J.P., and Chiocca, E.A. (2003). PTEN decreases in vivo vascularization of experimental gliomas in spite of proangiogenic stimuli. Cancer Res. *63*, 2300–2305.

Abrous, D.N., Koehl, M., and Le Moal, M. (2005). Adult neurogenesis: from precursors to network and physiology. Physiol. Rev. *85*, 523–569.

Anton, E.S., Ghashghaei, H.T., Weber, J.L., McCann, C., Fischer, T.M., Cheung, I.D., Gassmann, M., Messing, A., Klein, R., Schwab, M.H., et al. (2004). Receptor tyrosine kinase ErbB4 modulates neuroblast migration and placement in the adult forebrain. Nat. Neurosci. *7*, 1319–1328.

Bachoo, R.M., Maher, E.A., Ligon, K.L., Sharpless, N.E., Chan, S.S., You, M.J., Tang, Y., DeFrances, J., Stover, E., Weissleder, R., et al. (2002). Epidermal growth factor receptor and Ink4a/Arf: Convergent mechanisms governing terminal differentiation and transformation along the neural stem cell to astrocyte axis. Cancer Cell *1*, 269–277.

Balesaria, S., Brock, C., Bower, M., Clark, J., Nicholson, S.K., Lewis, P., de Sanctis, S., Evans, H., Peterson, D., Mendoza, N., et al. (1999). Loss of chromosome 10 is an independent prognostic factor in high-grade gliomas. Br. J. Cancer *81*, 1371–1377.

Bani-Yaghoub, M., Kendall, S.E., Moore, D.P., Bellum, S., Cowling, R.A., Nikopoulos, G.N., Kubu, C.J., Vary, C., and Verdi, J.M. (2004). Insulin acts as a myogenic differentiation signal for neural stem cells with multilineage differentiation potential. Development *131*, 4287–4298.

Barker, F.G., II, Davis, R.L., Chang, S.M., and Prados, M.D. (1996). Necrosis as a prognostic factor in glioblastoma multiforme. Cancer *77*, 1161–1166.

Berger, F., Gay, E., Pelletier, L., Tropel, P., and Wion, D. (2004). Development of gliomas: potential role of asymmetrical cell division of neural stem cells. Lancet Oncol. *5*, 511–514.

Broderick, D.K., Di, C., Parrett, T.J., Samuels, Y.R., Cummins, J.M., McLendon, R.E., Fults, D.W., Velculescu, V.E., Bigner, D.D., and Yan, H. (2004). Mutations of PIK3CA in anaplastic oligodendrogliomas, high-grade astrocytomas, and medulloblastomas. Cancer Res. *64*, 5048–5050.

Cairncross, J.G., Ueki, K., Zlatescu, M.C., Lisle, D.K., Finkelstein, D.M., Hammond, R.R., Silver, J.S., Stark, P.C., Macdonald, D.R., Ino, Y., et al. (1998). Specific genetic predictors of chemotherapeutic response and survival in patients with anaplastic oligodendrogliomas. J. Natl. Cancer Inst. *90*, 1473–1479.

Campos, L.S., Duarte, A.J., Branco, T., and Henrique, D. (2001). mDll1 and mDll3 expression in the developing mouse brain: role in the establishment of the early cortex. J. Neurosci. Res. *64*, 590–598.

Cao, L., Jiao, X., Zuzga, D.S., Liu, Y., Fong, D.M., Young, D., and During, M.J. (2004). VEGF links hippocampal activity with neurogenesis, learning and memory. Nat. Genet. *36*, 827–835.

Casarosa, S., Fode, C., and Guillemot, F. (1999). Mash1 regulates neurogenesis in the ventral telencephalon. Development *126*, 525–534.

Caussinus, E., and Gonzalez, C. (2005). Induction of tumor growth by altered stem-cell asymmetric division in Drosophila melanogaster. Nat. Genet. *37*, 1125.

Chakravarti, A., Zhai, G., Suzuki, Y., Sarkesh, S., Black, P.M., Muzikansky, A., and Loeffler, J.S. (2004). The prognostic significance of phosphatidylinositol 3-kinase pathway activation in human gliomas. J. Clin. Oncol. *22*, 1926–1933.

Chang, H.Y., Nuyten, D.S., Sneddon, J.B., Hastie, T., Tibshirani, R., Sorlie, T., Dai, H., He, Y.D., van't Veer, L.J., Bartelink, H., et al. (2005). Robustness, scalability, and integration of a wound-response gene expression signature in predicting breast cancer survival. Proc. Natl. Acad. Sci. USA *102*, 3738–3743.

Doetsch, F., Petreanu, L., Caille, I., Garcia-Verdugo, J.M., and Alvarez-Buylla, A. (2002). EGF converts transit-amplifying neurogenic precursors in the adult brain into multipotent stem cells. Neuron *36*, 1021–1034.

Eibl, R.H., Pietsch, T., Moll, J., Skroch-Angel, P., Heider, K.H., von Ammon, K., Wiestler, O.D., Ponta, H., Kleihues, P., and Herrlich, P. (1995). Expression of variant CD44 epitopes in human astrocytic brain tumors. J. Neurooncol. *26*, 165–170.

Fabel, K., Fabel, K., Tam, B., Kaufer, D., Baiker, A., Simmons, N., Kuo, C.J., and Palmer, T.D. (2003). VEGF is necessary for exercise-induced adult hippocampal neurogenesis. Eur. J. Neurosci. *18*, 2803–2812.

Fan, X., Mikolaenko, I., Elhassan, I., Ni, X., Wang, Y., Ball, D., Brat, D.J., Perry, A., and Eberhart, C.G. (2004). Notch1 and notch2 have opposite effects on embryonal brain tumor growth. Cancer Res. *64*, 7787–7793.

Fomchenko, E.I., and Holland, E.C. (2005). Stem cells and brain cancer. Exp. Cell Res. *306*, 323–329.

Freije, W.A., Castro-Vargas, F.E., Fang, Z., Horvath, S., Cloughesy, T., Liau, L.M., Mischel, P.S., and Nelson, S.F. (2004). Gene expression profiling of gliomas strongly predicts survival. Cancer Res. *64*, 6503–6510.

Galli, R., Binda, E., Orfanelli, U., Cipelletti, B., Gritti, A., De Vitis, S., Fiocco, R., Foroni, C., Dimeco, F., and Vescovi, A. (2004). Isolation and characterization of tumorigenic, stem-like neural precursors from human glioblastoma. Cancer Res. *64*, 7011–7021.

Godard, S., Getz, G., Delorenzi, M., Farmer, P., Kobayashi, H., Desbaillets, I., Nozaki, M., Diserens, A.C., Hamou, M.F., Dietrich, P.Y., et al. (2003). Classification of human astrocytic gliomas on the basis of gene expression: a correlated group of genes with angiogenic activity emerges as a strong predictor of subtypes. Cancer Res. *63*, 6613–6625.

Groszer, M., Erickson, R., Scripture-Adams, D.D., Lesche, R., Trumpp, A., Zack, J.A., Kornblum, H.I., Liu, X., and Wu, H. (2001). Negative regulation of neural stem/progenitor cell proliferation by the Pten tumor suppressor gene in vivo. Science *294*, 2186–2189.

Hartmann, C., Kluwe, L., Lucke, M., and Westphal, M. (1999). The rate of homozygous CDKN2A/p16 deletions in glioma cell lines and in primary tumors. Int. J. Oncol. *15*, 975–982.

Heimberger, A.B., Hlatky, R., Suki, D., Yang, D., Weinberg, J., Gilbert, M., Sawaya, R., and Aldape, K. (2005). Prognostic effect of epidermal growth factor receptor and EGFRvIII in glioblastoma multiforme patients. Clin. Cancer Res. *11*, 1462–1466.

Ho, D.M., Hsu, C.Y., Ting, L.T., and Chiang, H. (2003). MIB-1 and DNA topoisomerase IIα could be helpful for predicting long-term survival of patients with glioblastoma. Am. J. Clin. Pathol. *119*, 715–722.

Holland, E.C., Celestino, J., Dai, C., Schaefer, L., Sawaya, R.E., and Fuller, G.N. (2000). Combined activation of Ras and Akt in neural progenitors induces glioblastoma formation in mice. Nat. Genet. *25*, 55–57.

Hsu, S.C., Volpert, O.V., Steck, P.A., Mikkelsen, T., Polverini, P.J., Rao, S., Chou, P., and Bouck, N.P. (1996). Inhibition of angiogenesis in human glioblastomas by chromosome 10 induction of thrombospondin-1. Cancer Res. *56*, 5684–5691.

Ignatova, T.N., Kukekov, V.G., Laywell, E.D., Suslov, O.N., Vrionis, F.D., and Steindler, D.A. (2002). Human cortical glial tumors contain neural stem-like cells expressing astroglial and neuronal markers in vitro. Glia *39*, 193–206.

Jin, K., Zhu, Y., Sun, Y., Mao, X.O., Xie, L., and Greenberg, D.A. (2002). Vascular endothelial growth factor (VEGF) stimulates neurogenesis in vitro and in vivo. Proc. Natl. Acad. Sci. USA *99*, 11946–11950.

Kitange, G.J., Templeton, K.L., and Jenkins, R.B. (2003). Recent advances in the molecular genetics of primary gliomas. Curr. Opin. Oncol. *15*, 197–203.

Kleihues, P., and Cavenee, W.K. (2000). Pathology and Genetics of Tumours of the Nervous System (Lyon, France: IARC Press).

Knobbe, C.B., Merlo, A., and Reifenberger, G. (2002). Pten signaling in gliomas. Neuro-oncol. *4*, 196–211.

Ladi, E., Nichols, J.T., Ge, W., Miyamoto, A., Yao, C., Yang, L.-T., Boulter, J., Sun, Y.E., Kintner, C., and Weinmaster, G. (2005). The divergent DSL ligand Dll3 does not activate Notch signaling but cell autonomously attenuates signaling induced by other DSL ligands. J. Cell Biol. *170*, 983–992.

Liang, Y., Diehn, M., Watson, N., Bollen, A.W., Aldape, K.D., Nicholas, M.K., Lamborn, K.R., Berger, M.S., Botstein, D., Brown, P.O., and Israel, M.A. (2005). Gene expression profiling reveals molecularly and clinically distinct subtypes of glioblastoma multiforme. Proc. Natl. Acad. Sci. USA *102*, 5814–5819.

Ligon, K.L., Alberta, J.A., Kho, A.T., Weiss, J., Kwaan, M.R., Nutt, C.L., Louis, D.N., Stiles, C.D., and Rowitch, D.H. (2004). The oligodendroglial lineage marker OLIG2 is universally expressed in diffuse gliomas. J. Neuropathol. Exp. Neurol. *63*, 499–509.

Lin, H., Bondy, M.L., Langford, L.A., Hess, K.R., Delclos, G.L., Wu, X., Chan, W., Pershouse, M.A., Yung, W.K., and Steck, P.A. (1998). Allelic deletion analyses of MMAC/PTEN and DMBT1 loci in gliomas: relationship to prognostic significance. Clin. Cancer Res. *4*, 2447–2454.

Maurer, M.H., Tripps, W.K., Feldmann, R.E., Jr., and Kuschinsky, W. (2003). Expression of vascular endothelial growth factor and its receptors in rat neural stem cells. Neurosci. Lett. *344*, 165–168.

Mischel, P.S., Nelson, S.F., and Cloughesy, T.F. (2003). Molecular analysis of glioblastoma: pathway profiling and its implications for patient therapy. Cancer Biol. Ther. *2*, 242–247.

Misra, A., Pellarin, M., Nigro, J., Smirnov, I., Moore, D., Lamborn, K.R., Pinkel, D., Albertson, D.G., and Feuerstein, B.G. (2005). Array comparative genomic hybridization identifies genetic subgroups in grade 4 human astrocytoma. Clin. Cancer Res. *11*, 2907–2918.

Mizoguchi, M., Nutt, C.L., Mohapatra, G., and Louis, D.N. (2004). Genetic alterations of phosphoinositide 3-kinase subunit genes in human glioblastomas. Brain Pathol. *14*, 372–377.

Nakano, I., Paucar, A.A., Bajpai, R., Dougherty, J.D., Zewail, A., Kelly, T.K., Kim, K.J., Ou, J., Groszer, M., Imura, T., et al. (2005). Maternal embryonic leucine zipper kinase (MELK) regulates multipotent neural progenitor proliferation. J. Cell Biol. *170*, 413–427.

Newton, H.B. (2004). Molecular neuro-oncology and development of targeted therapeutic strategies for brain tumors. Part 2: PI3K/Akt/PTEN, mTOR, SHH/PTCH and angiogenesis. Expert Rev. Anticancer Ther. *4*, 105–128.

Nigro, J.M., Misra, A., Zhang, L., Smirnov, I., Colman, H., Griffin, C., Ozburn, N., Chen, M., Pan, E., Koul, D., et al. (2005). Integrated array-comparative genomic hybridization and expression array profiles identify clinically relevant molecular subtypes of glioblastoma. Cancer Res. *65*, 1678–1686.

Nutt, C.L., Mani, D.R., Betensky, R.A., Tamayo, P., Cairncross, J.G., Ladd, C., Pohl, U., Hartmann, C., McLaughlin, M.E., Batchelor, T.T., et al. (2003). Gene expression-based classification of malignant gliomas correlates better with survival than histological classification. Cancer Res. *63*, 1602–1607.

Okada, Y., Hurwitz, E.E., Esposito, J.M., Brower, M.A., Nutt, C.L., and Louis, D.N. (2003). Selection pressures of TP53 mutation and microenvironmental location influence epidermal growth factor receptor gene amplification in human glioblastomas. Cancer Res. *63*, 413–416.

Oliver, T.G., and Wechsler-Reya, R.J. (2004). Getting at the root and stem of brain tumors. Neuron *42*, 885–888.

Osada, H., Tokunaga, T., Nishi, M., Hatanaka, H., Abe, Y., Tsugu, A., Kijima, H., Yamazaki, H., Ueyama, Y., and Nakamura, M. (2004). Overexpression of the neuropilin 1 (NRP1) gene correlated with poor prognosis in human glioma. Anticancer Res. *24*, 547–552.

Parras, C.M., Galli, R., Britz, O., Soares, S., Galichet, C., Battiste, J., Johnson, J.E., Nakafuku, M., Vescovi, A., and Guillemot, F. (2004). Mash1 specifies neurons and oligodendrocytes in the postnatal brain. EMBO J. *23*, 4495–4505.

Pelloski, C.E., Mahajan, A., Maor, M., Chang, E.L., Woo, S., Gilbert, M., Colman, H., Yang, H., Ledoux, A., Blair, H., et al. (2005). YKL-40 expression is associated with poorer response to radiation and shorter overall survival in glioblastoma. Clin. Cancer Res. *11*, 3326–3334.

Phillips, H.S., Hains, J.M., Laramee, G.R., Rosenthal, A., and Winslow, J.W. (1990). Widespread expression of BDNF but not NT3 by target areas of basal forebrain cholinergic neurons. Science *250*, 290–294.

Pore, N., Liu, S., Haas-Kogan, D.A., O'Rourke, D.M., and Maity, A. (2003). PTEN mutation and epidermal growth factor receptor activation regulate vascular endothelial growth factor (VEGF) mRNA expression in human glioblastoma cells by transactivating the proximal VEGF promoter. Cancer Res. *63*, 236–241.

Prados, M.D., and Levin, V. (2000). Biology and treatment of malignant glioma. Semin. Oncol. *27*, 1–10.

Purow, B.W., Haque, R.M., Noel, M.W., Su, Q., Burdick, M.J., Lee, J., Sundaresan, T., Pastorino, S., Park, J.K., Mikolaenko, I., et al. (2005). Expression of Notch-1 and its ligands, Delta-like-1 and Jagged-1, is critical for glioma cell survival and proliferation. Cancer Res. *65*, 2353–2363.

Raab, S., Beck, H., Gaumann, A., Yuce, A., Gerber, H.P., Plate, K., Hammes, H.P., Ferrara, N., and Breier, G. (2004). Impaired brain angiogenesis and neuronal apoptosis induced by conditional homozygous inactivation of vascular endothelial growth factor. Thromb. Haemost. *91*, 595–605.

Radtke, F., and Clevers, H. (2005). Self-renewal and cancer of the gut: two sides of a coin. Science *307*, 1904–1909.

Rahaman, S.O., Harbor, P.C., Chernova, O., Barnett, G.H., Vogelbaum, M.A., and Haque, S.J. (2002). Inhibition of constitutively active Stat3 suppresses proliferation and induces apoptosis in glioblastoma multiforme cells. Oncogene *21*, 8404–8413.

Rajasekhar, V.K., Viale, A., Socci, N.D., Wiedmann, M., Hu, X., and Holland, E.C. (2003). Oncogenic Ras and Akt signaling contribute to glioblastoma formation by differential recruitment of existing mRNAs to polysomes. Mol. Cell *12*, 889–901.

Rao, R.D., Uhm, J.H., Krishnan, S., and James, C.D. (2003). Genetic and signaling pathway alterations in glioblastoma: relevance to novel targeted therapies. Front. Biosci. *8*, e270–e280.

Rickman, D.S., Bobek, M.P., Misek, D.E., Kuick, R., Blaivas, M., Kurnit, D.M., Taylor, J., and Hanash, S.M. (2001). Distinctive molecular profiles of high-grade and low-grade gliomas based on oligonucleotide microarray analysis. Cancer Res. *61*, 6885–6891.

Rietze, R.L., Valcanis, H., Brooker, G.F., Thomas, T., Voss, A.K., and Bartlett, P.F. (2001). Purification of a pluripotent neural stem cell from the adult mouse brain. Nature *412*, 736–739.

Sakamoto, M., Hirata, H., Ohtsuka, T., Bessho, Y., and Kageyama, R. (2003). The basic helix-loop-helix genes Hesr1/Hey1 and Hesr2/Hey2 regulate maintenance of neural precursor cells in the brain. J. Biol. Chem. *278*, 44808–44815.

Samuels, Y., Wang, Z., Bardelli, A., Silliman, N., Ptak, J., Szabo, S., Yan, H., Gazdar, A., Powell, S.M., Riggins, G.J., et al. (2004). High frequency of mutations of the PIK3CA gene in human cancers. Science *304*, 554.

Sanai, N., Tramontin, A.D., Quinones-Hinojosa, A., Barbaro, N.M., Gupta, N., Kunwar, S., Lawton, M.T., McDermott, M.W., Parsa, A.T., Manuel-Garcia Verdugo, J., et al. (2004). Unique astrocyte ribbon in adult human brain contains neural stem cells but lacks chain migration. Nature *427*, 740–744.

Schanzer, A., Wachs, F.P., Wilhelm, D., Acker, T., Cooper-Kuhn, C., Beck, H., Winkler, J., Aigner, L., Plate, K.H., and Kuhn, H.G. (2004). Direct stimulation of adult neural stem cells in vitro and neurogenesis in vivo by vascular endothelial growth factor. Brain Pathol. *14*, 237–248.

Schmidt, M.C., Antweiler, S., Urban, N., Mueller, W., Kuklik, A., Meyer-Puttlitz, B., Wiestler, O.D., Louis, D.N., Fimmers, R., and von Deimling, A. (2002). Impact of genotype and morphology on the prognosis of glioblastoma. J. Neuropathol. Exp. Neurol. *61*, 321–328.

Shen, Q., Goderie, S.K., Jin, L., Karanth, N., Sun, Y., Abramova, N., Vincent, P., Pumiglia, K., and Temple, S. (2004). Endothelial cells stimulate self-renewal and expand neurogenesis of neural stem cells. Science *304*, 1338–1340.

Shi, Y., Chichung Lie, D., Taupin, P., Nakashima, K., Ray, J., Yu, R.T., Gage, F.H., and Evans, R.M. (2004). Expression and function of orphan nuclear receptor TLX in adult neural stem cells. Nature *427*, 78–83.

Sieber-Blum, M. (2003). Ontogeny and plasticity of adult hippocampal neural stem cells. Dev. Neurosci. *25*, 273–278.

Simmons, M.L., Lamborn, K.R., Takahashi, M., Chen, P., Israel, M.A., Berger, M.S., Godfrey, T., Nigro, J., Prados, M., Chang, S., et al. (2001). Analysis of complex relationships between age, p53, epidermal growth factor receptor, and survival in glioblastoma patients. Cancer Res. *61*, 1122–1128.

Singh, S.K., Clarke, I.D., Terasaki, M., Bonn, V.E., Hawkins, C., Squire, J., and Dirks, P.B. (2003). Identification of a cancer stem cell in human brain tumors. Cancer Res. *63*, 5821–5828.

Singh, S.K., Hawkins, C., Clarke, I.D., Squire, J.A., Bayani, J., Hide, T., Henkelman, R.M., Cusimano, M.D., and Dirks, P.B. (2004). Identification of human brain tumour initiating cells. Nature *432*, 396–401.

Smith, J.S., Tachibana, I., Passe, S.M., Huntley, B.K., Borell, T.J., Iturria, N., O'Fallon, J.R., Schaefer, P.L., Scheithauer, B.W., James, C.D., et al. (2001). PTEN mutation, EGFR amplification, and outcome in patients with anaplastic astrocytoma and glioblastoma multiforme. J. Natl. Cancer Inst. *93*, 1246–1256.

Sonoda, Y., Ozawa, T., Aldape, K.D., Deen, D.F., Berger, M.S., and Pieper, R.O. (2001). Akt pathway activation converts anaplastic astrocytoma to glioblastoma multiforme in a human astrocyte model of glioma. Cancer Res. *61*, 6674–6678.

Stiles, B., Gilman, V., Khanzenzon, N., Lesche, R., Li, A., Qiao, R., Liu, X., and Wu, H. (2002). Essential role of AKT-1/protein kinase Bα in PTEN-controlled tumorigenesis. Mol. Cell. Biol. *22*, 3842–3851.

Su, J.D., Mayo, L.D., Donner, D.B., and Durden, D.L. (2003). PTEN and phosphatidylinositol 3′-kinase inhibitors up-regulate p53 and block tumor-induced angiogenesis: evidence for an effect on the tumor and endothelial compartment. Cancer Res. *63*, 3585–3592.

Tada, K., Shiraishi, S., Kamiryo, T., Nakamura, H., Hirano, H., Kuratsu, J., Kochi, M., Saya, H., and Ushio, Y. (2001). Analysis of loss of heterozygosity on chromosome 10 in patients with malignant astrocytic tumors: correlation with patient age and survival. J. Neurosurg. *95*, 651–659.

Tanwar, M.K., Gilbert, M.R., and Holland, E.C. (2002). Gene expression microarray analysis reveals YKL-40 to be a potential serum marker for malignant character in human glioma. Cancer Res. *62*, 4364–4368.

Tumor Analysis Best Practices Working Group. (2004). Expression profiling—best practices for data generation and interpretation in clinical trials. Nat. Rev. Genet. *5*, 229–237.

Uhrbom, L., Dai, C., Celestino, J.C., Rosenblum, M.K., Fuller, G.N., and Holland, E.C. (2002). Ink4a-Arf loss cooperates with KRas activation in astrocytes and neural progenitors to generate glioblastomas of various morphologies depending on activated Akt. Cancer Res. *62*, 5551–5558.

Ushio, Y., Tada, K., Shiraishi, S., Kamiryo, T., Shinojima, N., Kochi, M., and Saya, H. (2003). Correlation of molecular genetic analysis of p53, MDM2, p16, PTEN, and EGFR and survival of patients with anaplastic astrocytoma and glioblastoma. Front. Biosci. *8*, e281–e288.

van den Boom, J., Wolter, M., Kuick, R., Misek, D.E., Youkilis, A.S., Wechsler, D.S., Sommer, C., Reifenberger, G., and Hanash, S.M. (2003). Characterization of gene expression profiles associated with glioma progression using oligonucleotide-based microarray analysis and real-time reverse transcription-polymerase chain reaction. Am. J. Pathol. *163*, 1033–1043.

von Deimling, A., Louis, D.N., and Wiestler, O.D. (1995). Molecular pathways in the formation of gliomas. Glia *15*, 328–338.

Watanabe, K., Tachibana, O., Sata, K., Yonekawa, Y., Kleihues, P., and Ohgaki, H. (1996). Overexpression of the EGF receptor and p53 mutations are mutually exclusive in the evolution of primary and secondary glioblastomas. Brain Pathol. *6*, 217–223.

Weng, A.P., Ferrando, A.A., Lee, W., Morris, J.P., IV, Silverman, L.B., Sanchez-Irizarry, C., Blacklow, S.C., Look, A.T., and Aster, J.C. (2004). Activating mutations of NOTCH1 in human T cell acute lymphoblastic leukemia. Science *306*, 269–271.

Wurmser, A.E., Nakashima, K., Summers, R.G., Toni, N., D'Amour, K.A., Lie, D.C., and Gage, F.H. (2004). Cell fusion-independent differentiation of neural stem cells to the endothelial lineage. Nature *430*, 350–356.

Xiao, A., Yin, C., Yang, C., Di Cristofano, A., Pandolfi, P.P., and Van Dyke, T. (2005). Somatic induction of Pten loss in a preclinical astrocytoma model reveals major roles in disease progression and avenues for target discovery and validation. Cancer Res. *65*, 5172–5180.

Yasuhara, T., Shingo, T., and Date, I. (2004). The potential role of vascular endothelial growth factor in the central nervous system. Rev. Neurosci. *15*, 293–307.

Yoon, K., and Gaiano, N. (2005). Notch signaling in the mammalian central nervous system: insights from mouse mutants. Nat. Neurosci. *8*, 709–715.

Zhu, Y., Jin, K., Mao, X.O., and Greenberg, D.A. (2003). Vascular endothelial growth factor promotes proliferation of cortical neuron precursors by regulating E2F expression. FASEB J. *17*, 186–193.

Zhu, Y., Guignard, F., Zhao, D., Liu, L., Burns, D.K., Mason, R.P., Messing, A., and Parada, L.F. (2005). Early inactivation of p53 tumor suppressor gene cooperating with NF1 loss induces malignant astrocytoma. Cancer Cell *8*, 119–130.

Accession numbers

The microarray data have been submitted to Gene Expression Omnibus (GEO), and the accession number for the data series is GSE4271.